ACS Synthetic Biology

pubs.acs.org/synthbio

Research Article

A BioBricks Metabolic Engineering Platform for the Biosynthesis of Anthracyclinones in *Streptomyces coelicolor*

Rongbin Wang,[¶] Jennifer Nguyen,[¶] Jacob Hecht, Nora Schwartz, Katelyn V. Brown, Larissa V. Ponomareva, Magdalena Niemczura, Dino van Dissel, Gilles P. van Wezel, Jon S. Thorson, Mikko Metsä-Ketelä,* Khaled A. Shaaban,* and S. Eric Nybo*

Cite This: *ACS Synth. Biol.* 2022, 11, 4193−4209

Read Online

ACCESS | Metrics & More | Article Recommendations | Supporting Information

ABSTRACT: Actinomycetes produce a variety of clinically indispensable molecules, such as antineoplastic anthracyclines. However, the actinomycetes are hindered in their further development as genetically engineered hosts for the synthesis of new anthracycline analogues due to their slow growth kinetics associated with their mycelial life cycle and the lack of a comprehensive genetic toolbox for combinatorial biosynthesis. In this report, we tackled both issues via the development of the BIOPOLYMER (BIOBricks POLYketide Metabolic EngineeRing) toolbox: a comprehensive synthetic biology toolbox consisting of engineered strains, promoters, vectors, and biosynthetic genes for the synthesis of anthracyclinones. An improved derivative of the production host *Streptomyces coelicolor* M1152 was created by deleting the *matAB* gene cluster that specifies extracellular poly-β-1,6-*N*-acetylglucosamine (PNAG). This resulted in a loss of mycelial aggregation, with improved biomass accumulation and anthracyclinone production. We then leveraged BIOPOLYMER to engineer four distinct anthracyclinone pathways, identifying optimal combinations of promoters, genes, and vectors to produce aklavinone, 9-*epi*-aklavinone, auramycinone, and nogalamycinone at titers between 15−20 mg/L. Optimization of nogalamycinone production strains resulted in titers of 103 mg/L. We structurally characterized six anthracyclinone products from fermentations, including new compounds 9,10-*seco*-7-deoxy-nogalamycinone and 4-*O*-β-D-glucosyl-nogalamycinone. Lastly, we tested the antiproliferative activity of the anthracyclinones in a mammalian cancer cell viability assay, in which nogalamycinone, auramycinone, and aklavinone exhibited moderate cytotoxicity against several cancer cell lines. We envision that BIOPOLYMER will serve as a foundational platform technology for the synthesis of designer anthracycline analogues.

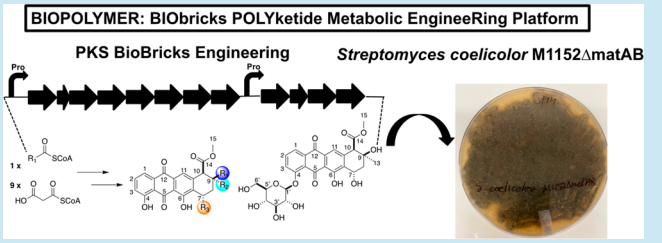

KEYWORDS: *BioBricks, synthetic biology, natural product biosynthesis, anthracyclinones, Streptomyces coelicolor, anticancer*

Downloaded via UNIV OF TURKU on January 3, 2023 at 06:35:12 (UTC).
See https://pubs.acs.org/sharingguidelines for options on how to legitimately share published articles.

INTRODUCTION

Anthracyclines are clinically important natural products for the treatment of human cancers.[1] Anthracyclines influence DNA and chromatin structure via two distinct mechanisms: histone eviction from open chromosomal regions and the inhibition of topoisomerase II, resulting in the formation of double-stranded DNA breaks.[2] Recently, several anthracycline biosynthetic pathways have been characterized, which provide genetic tools for the metabolic engineering of new anthracycline derivatives. The nogalamycin, aclacinomycin, and daunorubicin polyketide pathways are canonical examples of anthracycline biosynthesis and have been studied in detail over the past few decades.[3−7] For example, anthracyclinones are C_{20} (e.g., nogalamycin) or C_{21} (e.g., daunorubicin or aclacinomycin) aromatic polyketides that are synthesized by minimal polyketide synthase (minPKS) composed of a ketoacyl synthase (KSa, AknB/DpsA/Snoa1), chain length factor (KSb, AknC/DpsB/Snoa2), and an acyl carrier protein (ACP, AknD/DpsG/Snoa3) to form an enzyme-linked poly-β-ketothioester intermediate (Figure 1). The AknBCDE2F or DpsABCDG minPKS complex condenses one propionyl-CoA starter unit to nine malonyl-CoA extender units to form a C-21 intermediate,[8] whereas the Snoa123 minPKS condenses one acetyl-CoA and nine malonyl-CoA extender units to form a C-20 polyketide. The poly-β-ketothioester is reduced at 9-position by a PKS-associated ketoreductase (KR, AknA/DpsE/SnoaD), and then is aromatized via C7−C12 cyclization (ARO, AknE/DpsF/SnoaE), C5−C14 and C3−C16 cyclization via second-third ring cyclase (CYC, AknW/DpsY/SnoaM),[9] and C-12 oxidation via an anthraquinol oxygenase (OXY, AknX/DpsG/SnoaB)[10] to afford a tricyclic anthraquinone intermediate (Figure 1). The tricyclic anthracyclinone is *O*-methylated to form nogalonic acid methyl ester (NAME,

Received: September 15, 2022
Published: November 15, 2022

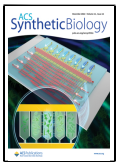

© 2022 The Authors. Published by American Chemical Society

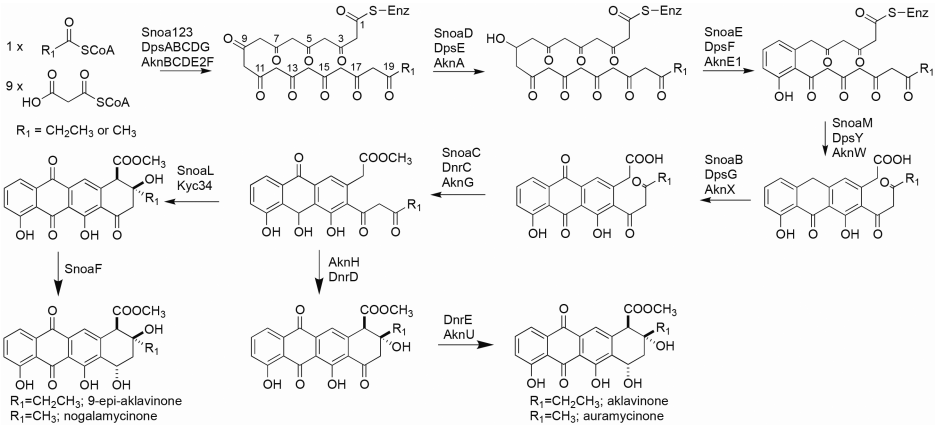

Figure 1. Biosynthesis of anthracyclinones. One acetyl-CoA or propionyl-CoA starter unit is condensed with nine malonyl-CoA extender units via iterative Claisen condensation reactions via the minimal PKS to form an enzyme-tethered decaketide intermediate. The polyketide ketoreductase reduces the 9-ketone to a hydroxyl group followed by C7−C12 first-ring aromatization, C5−C14 s-ring cyclization, and C3−C16 third-ring cyclization by the second-third ring cyclase. C-12 oxidation is catalyzed by an anthraquinol monooxygenase, followed by *O*-methylation to afford a tricyclic anthraquinone methyl ester. The key tricyclic intermediate undergoes fourth-ring cyclization via two distinct routes: SnoaL/Kyc34 cyclizes the fourth ring to afford a 9(*S*)-anthracyclinone and AknH/DnrD cyclizes the fourth ring to afford a 9(*R*)-anthracyclinone. The final step is C-7 ketoreduction by ketoreductases to afford C-21 anthracyclinones 9-*epi*-aklavinone or aklavinone and C-20 anthracyclinones nogalamycinone and auramycinone.

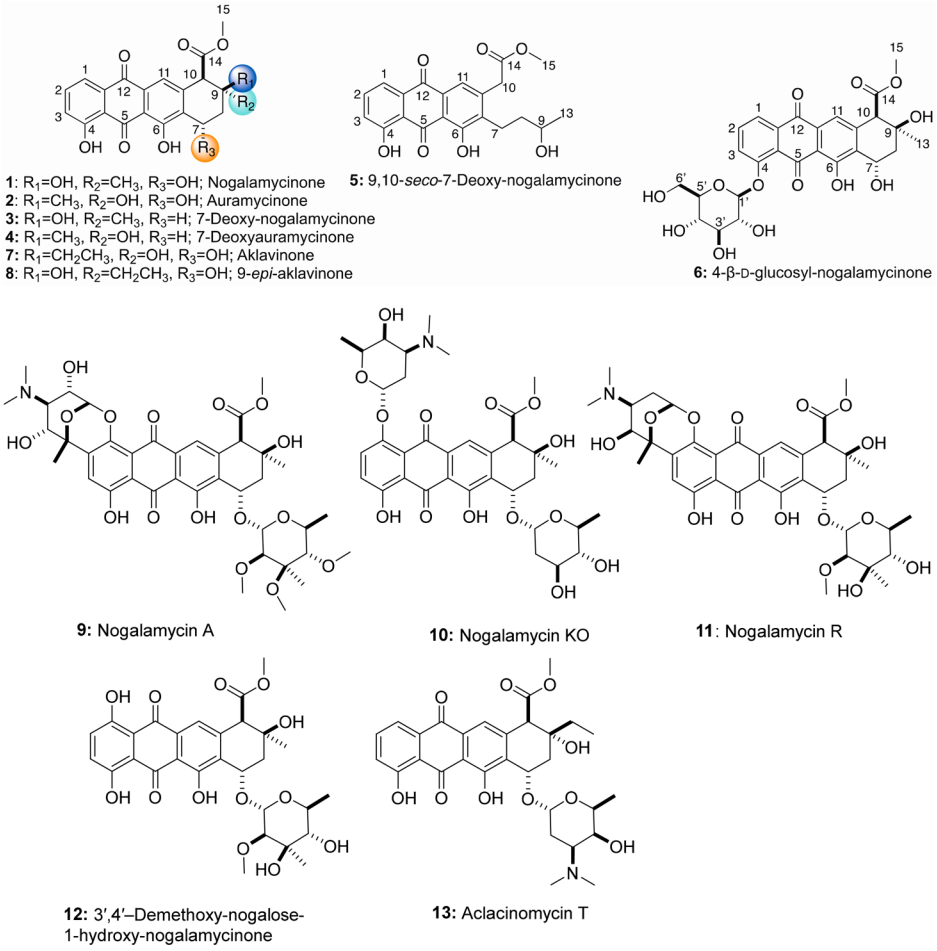

Figure 2. Structures of anthracyclin(on)es described in this work.

SnoaC)[11] or aklanonic acid methyl ester (AAME, AknG/DnrC),[12] respectively, followed by fourth-ring cyclization to a 9(*S*)-configured anthracyclinone (Kyc34/SnoaL) and subsequent C7-ketoreduction (SnoaF) to afford nogalamycinone or 9-*epi*-aklavinone[13,14] (Figure 1). Alternatively, the tricyclic intermediate can undergo fourth-ring cyclization to a 9(*R*)-configured anthracyclinone (AknH/DnrD) and 7-ketoreduction (AknU/DnrE) to yield aklavinone or auramycinone (Figure 1).[15] Inspired by the biosynthetic logic of the anthracycline PKS system, the motivation for the present work was to develop an

https://doi.org/10.1021/acssynbio.2c00498
ACS Synth. Biol. 2022, 11, 4193−4209

Table 1. Plasmids Constructed and/or Used in This Study

plasmid	genotype and relevant characteristics	reference
pSET152	*aac3(IV)*, *oriT*, *lacZα*, ΦC31int, *attP*, MCS	[26]
pSET152BB	BioBricks-compatible vector pSET152; $aac3(IV)^R$, *oriT*, *ϕ*C31int, *attP*, MCS	[24]
pENSV1	BioBricks-compatible vector; $aadA^R$, bla^R, *oriT*, *ϕ*SV1int, *attP*	[24]
pENTG1	BioBricks-compatible vector; vph^R, bla^R, *oriT*, *ϕ*TG1int, *attP*	[24]
pOSV808	BioBricks-compatible vector; hph^R, *oriT*, VWBint, *attP*, *amilCFP*	[32]
pSnogaori	pKC505-based *E. coli*−*Streptomyces* shuttle vector harboring 30.26 kb fragment of nogalamycin biosynthetic gene cluster; *aac(3)IV*, *SCP2* ori*, pBR322 *ori*, *λ* cos sites	Accession No. OM832358,[33]
pSET154BB	pSET152BB with strong 5′-*tt-sbi-A* terminator and 3′-*fd* phage terminator	This study,[8,9]
pENSV3	pENSV1 with strong 5′- ECK120010818-term and 3′- ECK120029600-spy-term terminators	This study,[10]
pENTG3	pENTG1 with strong 5′- L3S2P21-term and 3′- L3S3P41-term terminators	This study,[10]
pSET-S1	wild-type *snoa123* fused to the medium *ermE*p* promoter; cloned in pSET152BB vector	This study
pSET-S2	wild-type *snoa123* fused to the strong *kasOp** promoter; cloned in pSET152BB vector	This study
pSET-S3	codon-optimized *snoa123* fused to the strong *kasOp** promoter; cloned in pSET152BB vector	This study
pSET-A1	wild-type *aknBCDE2F* fused to the medium *ermE*p* promoter; cloned in pSET152BB vector	This study
pSET-A2	wild-type *aknBCDE2F* fused to the strong *kasOp** promoter; cloned in pSET152BB vector	This study
pSET-D1	wild-type *dpsABCDG* fused to the medium *ermE*p* promoter; cloned in pSET152BB vector	This study
pSET-D2	wild-type *dpsABCDG* fused to the medium *kasOp** promoter; cloned in pSET152BB vector	This study
pSET-O2	wild-type *oxyABCD* fused to the strong *kasOp** promoter; cloned in pSET152BB	This study
pSET-S2S5	*kasOp*-snoa123+kasOp*-snoaDEMB* cloned in pSET152BB	This study
pSET-D1S5	*ermE*p-dpsABCDG+kasOp*-snoaDEMB* cloned in pSET152BB	This study
pSET-D2S5	*kasOp*-dpsABCDG+kasOp*-snoaDEMB* cloned in pSET152BB	This study
pSET-A1S5	*ermE*p-aknBCDE2F+kasOp*-snoaDEMB* cloned in pSET152BB	This study
pSET-A1S5	*kasOp*-aknBCDE2F+kasOp*-snoaDEMB* cloned in pSET152BB	This study
pSET-D1D5	*ermE*p-dpsABCDG+kasOp*-dpsEFYdnrG* cloned in pSET152BB	This study
pSET-D2D5	*kasOp*-dpsABCDG+kasOp*-dpsEFYdnrG* cloned in pSET152BB	This study
pSET-A1D5	*ermE*p-aknBCDE2F+kasOp*-dpsEFYdnrG* cloned in pSET152BB	This study
pSET-A2D5	*kasOp* -aknBCDE2F+kasOp*-dpsEFYdnrG* cloned in pSET152BB	This study
pSET-D1A5	*ermE*p-dpsABCDG+kasOp*-aknAE1WX* cloned in pSET152BB	This study
pSET-D2A5	*kasOp*-dpsABCDG+kasOp*-aknAE1WX* cloned in pSET152BB	This study
pSET-A1A5	*ermE*p-aknBCDE2F+kasOp*-aknAE1WX* cloned in pSET152BB	This study
pSET-A2A5	*kasOp*-aknBCDE2F+kasOp*-aknAE1WX* cloned in pSET152BB	This study
pSV-S4	*kasOp*-snoaDEM* cloned in pENSV1	This study
pSV-S5	*kasOp*-snoaDEMB* cloned in pENSV1	This study
pSV-A4	*kasOp*-aknAE1W* cloned in pENSV1	This study
pSV-A5	*kasOp*-aknAE1WX* cloned in pENSV1	This study
pTG-S6	*sp44-snoaLCF* cloned in pENTG1	This study
pTG-S7	*sp44-snoaC+kyc34+snoaF* cloned in pENTG1	This study
pTG-A6	*sp44-aknGHU* cloned in pENTG1	This study
pTG-D6	*sp44-dnrCDE* cloned in pENTG1	This study
pEN10001	*kasOp*-aknBCDE2F+kasOp*-aknAE1WX+sp44-aknGHU* cloned into pSET154BB	This study
pEN10002	*kasOp*-aknBCDE2F+kasOp*-aknAE1WX+sp44-snoaC+kyc34+snoaF* cloned into pSET154BB	This study
pEN10003	*kasOp*-snoa123+kasOp*-snoaDEMB+sp44-aknGHU* cloned into pSET154BB	This study
pEN10004	*kasOp*-snoa123+kasOp*-snoaDEMB+sp44-snoaC+kyc34+snoaF*	This study
pRW10000	codon-optimized *kasOp*-snoa123+kasOp*-aknAE1WX+sp44-snoaLCF*	This study

expanded metabolic engineering toolset to improve access to these important natural products and to generate new anthracycline analogues via microbial synthesis.

Synthetic biology is a discipline that has been defined as the "engineering-driven building of increasingly complex biological entities for novel applications".[16] Indeed, the field of synthetic biology has resulted in new genetic systems and organisms useful for filling in critical gaps in the pharmaceutical, biofuels, and cosmetics industries.[17] Synthetic biology boasts the development of a variety of genetic tools, including chassis hosts, promoters, terminators, genes, and vectors useful for reprogramming model organisms. Synthetic biology is also a promising discipline for increasing access to indispensable natural products, such as polyketides.[18] Synthetic biology has also contributed new tools for the refinement of idiosyncratic model organisms, such as *Streptomyces* spp., that are difficult to transform or feature morphological limitations, such as the formation of mycelial clumps during submerged liquid fermentation.[19,20] *Streptomyces* produce valuable bioactive molecules, such as anthracyclines and tetracyclines. *Streptomyces* spp. exhibit a highly complex life cycle, including sporulation, branching, fragmentation, and adhesion that is regulated and correlated with specialized metabolism, which limits their use as industrial hosts. Recently, the *matAB* gene cluster was discovered to encode novel glycosyltransferases responsible for the synthesis of extracellular poly-*β*-1,6-*N*-acetylglucosamine (PNAG) that leads to cellular clumping.[21] Van Dissel et al. inactivated the *matAB* gene cluster in *Streptomyces coelicolor* M145 and characterized strains that lost the mycelial aggregation phenotype and exhibited improved biomass accumulation. Here, we developed the derivative strain *Streptomyces coelicolor* M1152Δ*matAB* as an improved cell

https://doi.org/10.1021/acssynbio.2c00498
ACS Synth. Biol. 2022, 11, 4193−4209

factory for the metabolic engineering of minimal aromatic polyketides from type II PKS pathways.

In this report, we developed a BioBricks toolkit of promoters, expression vectors, and engineered *Streptomyces* hosts for the metabolic engineering of anthracyclinones from type II PKS pathways. All genes were assembled according to the BioBricks [RFC10] standard. We designed minimal PKS (minPKS) cassettes based on the *snoa123* (C-20 nogalamycin), *aknBC-DE2F* (C-21 aclacinomycin), *dpsABGCD* (C-21 doxorubicin), and *oxyABCD* (C-19N oxytetracycline) biosynthetic pathways. First, we compared the production titer resulting from expressing minPKS gene cassettes in different Streptomyces hosts: *Streptomyces lividans* K4−114, *Streptomyces coelicolor* M1146, M1152, and M1154, and *Streptomyces coelicolor* M1152Δ*matAB*. These experiments resulted in the production of the expected aromatic minimal polyketides. Second, we performed combinatorial biosynthesis experiments by coexpressing the minPKS gene cassettes with different combinations of KR/ARO/CYC/OXY genes to optimize metabolic flux toward tricyclic anthracyclinones. Third, we coexpressed different orthologs of *O*-methyltransferases, fourth ring cyclases, and 7-ketoreductases to generate the expected anthracyclinones. Finally, the optimum gene combinations were cloned onto one plasmid to determine the production yields in *S. coelicolor* M1152Δ*matAB*. This work resulted in the production of eight anthracyclinone analogues, including the new compounds 9,10-*seco*-7-deoxy-nogalamycinone and 4-β-D-glucosyl-nogalamycinone and the unexpected 7-deoxy analogues (Figure 2). Finally, the anticancer activity of the different anthracyclinone derivatives was assessed in a mammalian cell viability assay, which revealed that nogalamycinone, auramycinone, and aklavinone had moderate antiproliferative activity (<30 μM IC_{50}) against several human cancer cell lines.

RESULTS AND DISCUSSION

Engineering of the *snoa123* MinPKS into Different *Streptomyces* spp. Hosts. We first synthesized a codon-optimized version of the *Streptomyces nogalater* minimal polyketide synthase (*snoa123*) responsible for the synthesis of the nogalamycin C-20 poly-β-ketothioester (Figure 1). The codon optimization was based on the native codon preference for *S. coelicolor* (Genscript, OptimumGene). Previously, the involvement of *snoa123* in the synthesis of nogalamycin has been confirmed via heterologous expression studies and genetic complementation studies in *Streptomyces* spp. strains.[6,22] The *snoa123* operon was designed based on principles from the BioBricks [RFC-10] standard: (1) the genes were decoupled from their native translational coupling and synthesized as individual ORFs; (2) the strong BBa_B0034 ribosome binding site was incorporated into the 5′-untranslated region (5′-AAAGAGGAGAAA-3′) to control the rate of translation initiation for each gene in the operon;[23,24] (3) the genes were cloned to lack internal *Eco*RI, *PstI*, *SpeI*, and *XbaI* restriction sites, and if necessary, silent mutations were engineered in these restriction sites to make the genes compatible with the BioBricks [RFC-10] standard; (4) the genes were given BioBricks prefix (5′-GAATTCGCGGCCGCTTCTAGAG-3′) and suffix (5′-TACTAGTAGCGGCCGCTGCAG-3′) sequences to enable isocaudomer cloning[25] (Table 1). To facilitate gene expression, we generated a BioBricks compatible version of the ϕC31-based integrating expression vector pSET152[26] (e.g., pSET152BB) to allow for cloning into *Eco*RI/*PstI* sites and transformation into *S. coelicolor* via intergeneric conjugation (Table 1).[27] The genes were expressed from the strong constitutive promoter *kasOp**.[28,29] The resulting pSET152BB derivative featured the *snoa123* fused to the *kasOp** promoter and was transformed into three heterologous hosts: (1) *S. lividans* K4−114 (lacking the actinorhodin type II polyketide synthase gene cluster);[30] (2) *S. coelicolor* M1146 (lacking the prodiginine, actinorhodin, coelimycin, and cryptic polyketide gene clusters);[31] and (3) *S. coelicolor* M1152 (an RNA polymerase B up-regulated mutant of *S. coelicolor* M1146) (Table 2).

Table 2. Bacterial Strains Used in This Study

strain	genotype or comments	source or reference
Escherichia coli JM109	F′ *traD36 proA+B+lacIq* Δ(*lacZ*)M15/ Δ(*lac-proAB*) *gln V44 e14- gyrA96 recA1 relA1 endA1 thi hsdR17*	Promega
Escherichia coli ET12567/ (pUZ8002)	*dam- dcm- hsdM hsdS hsdR cat tet*; carrying plasmid pUZ8002	34
Streptomyces lividans K4−114	*pro-2 str-6 SLP2- SLP3- act::ermE*	30
Streptomyces coelicolor M1146	SCP1- SCP2- Δ*act* Δ*red* Δ*cpk* Δ*cda*	31
Streptomyces coelicolor M1152	SCP1- SCP2- Δ*act* Δ*red* Δ*cpk* Δ*cda* *rpoB*(C1298T)	31
Streptomyces coelicolor M1152Δ*matAB*	SCP1- SCP2- Δ*act* Δ*red* Δ*cpk* Δ*cda* *rpoB*(C1298T) Δ*sco2961−2962*	This study,[19]

The heterologous expression of the codon-optimized *snoa123* operon resulted in significant production of yellow-orange pigments on SFM agar plates. Each of the recombinant strains was plated in triplicate on R5 agar plates for 5 days and then extracted to analyze the production of polyketides (Figure 3). Each strain produced copious amounts of known polyketides SEK15 (e.g., $C_{20}H_{16}O_8$, calc. m/z = 385.0923 $[M + H]^+$; found m/z = 385.0910 $[M + H]^+$) and SEK15b (e.g., $C_{20}H_{12}O_8$, calc. m/z = 381.0610 $[M + H]^+$; found m/z = 381.0595 $[M + H]^+$) as determined by HRESI-MS analysis (Supporting Information Figures S11 and S12). *S. lividans* K4−114 also produced large quantities of undesired prodiginines, based on HRESI-MS total ion counts, and therefore this strain was excluded from further experimentation. The production titer of SEK15 was strain-dependent and media-dependent. On R5 agar plates, the strains transformed with empty pSET152BB vector produced no detectable SEK15; however, *S. lividans* K4−114 expressing the construct produced 39.6 mg/L SEK15, *S. coelicolor* M1146 produced 39.7 mg/L SEK15, and *S. coelicolor* M1152 produced 34.8 mg/L SEK15 (Figure 3). In SG liquid media, *S. coelicolor* M1146 and M1152 strains transformed with empty pSET152BB produced no SEK15, whereas *S. coelicolor* M1152 expressing the *snoa123* operon produced 55 mg/L SEK15 and *S. coelicolor* M1146 produced the highest SEK15 titer at 79 mg/L (Figure 3).

Engineering of *aknBCDE2F*, *dpsABCDG*, and *oxyABCD* MinPKS Operons into *S. coelicolor*. To compare the biosynthetic capacity of *S. coelicolor* M1152 and the *S. coelicolor* M1152Δ*matAB* mutant, heterologous expression experiments were conducted to produce minimally cyclized aromatic polyketides using propionyl-CoA, acetyl-CoA, or malonamyl-CoA starter units. We anticipated that the strains resulting from these experiments would serve as a proof-of-concept for the use of *S. coelicolor* M1152Δ*matAB* as a production host for pathway engineering of anthracyclines. The original *aknBCDE2F* gene annotations from *Streptomyces galilaeus* ATCC 31615 (Accession No. AF257324.2) were revised using next-generation

https://doi.org/10.1021/acssynbio.2c00498
ACS Synth. Biol. 2022, 11, 4193−4209

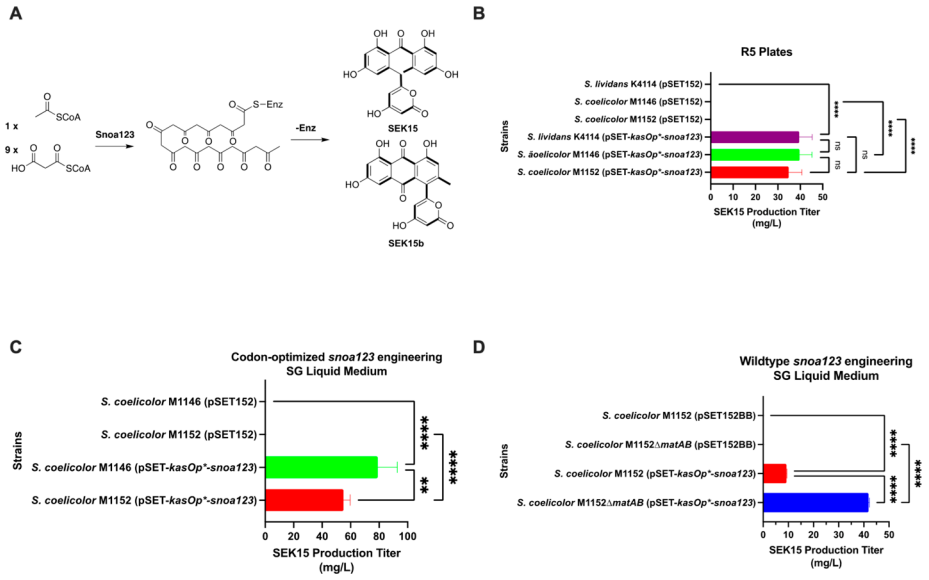

Figure 3. Metabolic engineering of SEK15. (A) Scheme for the biosynthesis of SEK15 via the Snoa123 minPKS. (B) Production titers of SEK15 on R5 solid agar plates from the heterologous expression of codon-optimized *snoa123* in *S. lividans* K4−114, *S. coelicolor* M1146, and *S. coelicolor* M1152. (C) Production titers of SEK15 in SG liquid media shake flask experiments from the heterologous expression of codon-optimized *snoa123* in *S. coelicolor* M1146 and *S. coelicolor* M1152. (D) Production titers of SEK15 in SG liquid media shake flask experiments from the heterologous expression of wild-type *snoa123* in *S. coelicolor* M1152 and *S. coelicolor* M1152Δ*matAB*. Experiments were carried out in double triplicate and the error bars reflect the standard deviation. ANOVA was carried out to determine the statistical significance between strains. The statistically significant comparisons are reflected with asterisks. The statistical significance of observed results was established with a $p < 0.05$. * indicates $p \leq 0.05$, ** indicates $p \leq 0.01$, *** indicates $p \leq 0.001$, and **** indicates $p \leq 0.0001$.

sequencing (Supporting Information, Table S1). Next-generation sequencing of pSnogaori, which encodes the majority of the nogalamycin biosynthetic pathway, identified several mutations in the original annotations of *snoaD*, *snoaE*, *snoaM*, and *snoaB* genes. The revised sequence was deposited in the NCBI database (Accession No. OM832358). Despite several attempts to express codon-optimized versions of the *aknBC-DE2F*, *dpsABCDG*, and *oxyABCD* minPKS operons, attempts to produce the expected minimal aromatic polyketides were unsuccessful. These attempts also included the preservation of the native translational coupling and ribosome binding site of the KS*α*-KS*β* subunits, which Liu et al. previously demonstrated to be indispensable for the expression of the *alpABC* and *whiE−III−IV−V* type II PKS subunits in *E. coli*.[35] As a result, we focused further construct development on the expression of wild-type versions of the *snoa123*, *aknBCDE2F*, *dpsABCDG*, and *oxyABCD* minPKS operons.[36] The expression of *aknBCDE2F* and *dpsABCDG* operons was expected to produce the C-21 polyketide UWM7 and the *oxyABCD* operon was expected to produce the amidated polyketide WJ85.[37,38] We cloned the *aknBCDE2F*, *snoa123*, and *oxyABCD* genes under the control of the intermediate strength *ermE*p* promoter or the strong *kasOp** promoter and spliced these cassettes into pSET152BB.[28,39] The resulting plasmids were transformed into *S. coelicolor* M1152 and *S. coelicolor* M1152Δ*matAB* via intergeneric conjugation. *S. coelicolor* M1152/pSET152BB and *S. coelicolor* M1152Δ*matAB*/pSET152BB were included in the analysis as negative controls.

Expression of the wild-type *snoa123* minPKS in *S. coelicolor* M1152 resulted in the production of 9.2 mg/L SEK15, *S. coelicolor* M1152ΔmatAB harboring the same construct produced 3-fold more SEK15 at 41.8 mg/L ($p < 0.0001$) (Figure 3). The codon-optimized version of *snoa123* was more productive than the wild-type version of *snoa123* (e.g., 79 mg/L), which indicates that codon-optimization likely enhances translation of the Snoa123 minPKS complex and results in greater metabolic flux toward SEK15 via mass action. We previously observed a similar result when comparing wild-type and codon-optimized versions of the valerena-1,10-diene synthase, *VoTPS1*, in *E. coli*.[40] Expression of the codon-optimized version resulted in a 3-fold greater production titer of valerena-1,10-diene than the wild-type version. Additionally, this result demonstrates that the dispersed growth phenotype of *S. coelicolor* M1152Δ*matAB* greatly enhanced polyketide production.

We are only beginning to unravel the mechanisms that control morphogenesis of streptomycetes in submerged cultures. Productivity of streptomycetes in industrial fermentation depends on the mycelial morphology in a product-dependent manner; in other words, less favorable growth conditions may have to be accepted to obtain good productivity.[41−44] Considering that it is hard to predict how production responds to changes in growth and morphology, we need to have more tools at our disposal to change the growth characteristics and thus optimize the chance of success. Overexpression of the cell division activator SsgA increases fragmentation of streptomycetes, which leads to faster growth. A strain of *S. coelicolor* overexpressing SsgA produced large amounts of prodigionines, but hardly any actinorhodin.[45] However, SsgA affects the intracellular architecture, making the hyphae less robust. Deletion of *matAB* prevents the production of poly-*N*-acetylglucosamine (PNAG), an EPS that "glues" the hyphae together, promoting pellet formation.[19,21] Deletion of *matAB* in *S. coelicolor* M1152 significantly resulted in a dispersed growth phenotype (data not shown) and led to better productivity. The more PNAG is produced the larger the pellets, and thus the technology may be widely applicable.

https://doi.org/10.1021/acssynbio.2c00498
ACS Synth. Biol. 2022, 11, 4193−4209

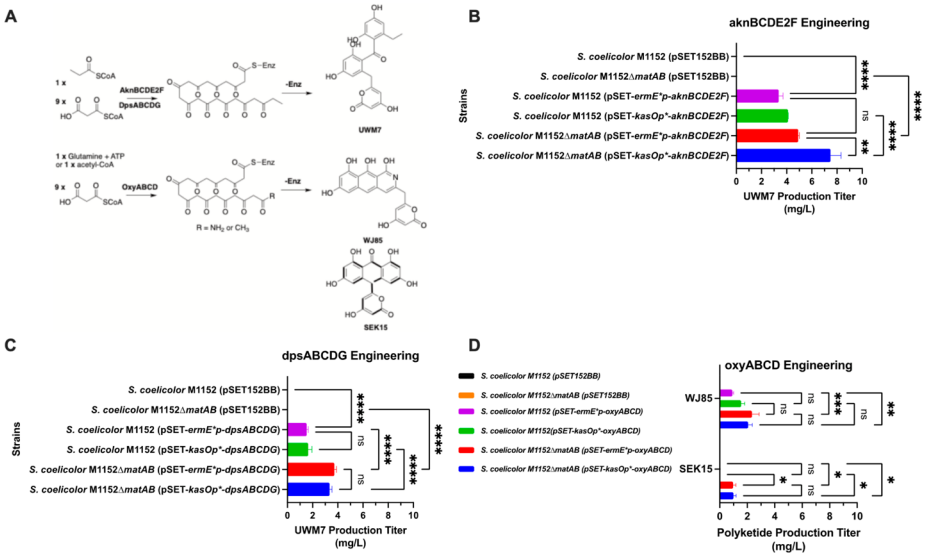

Figure 4. Engineering of UWM7 and WJ85 minimal aromatic polyketides. (A) Biosynthesis scheme for the synthesis of UWM7 from the DpsABCDG/AknBCDE2F minPKS and WJ85 from the OxyABCD minPKS. (B) Production titers of UWM7 resulting from the engineering of pSET-*ermE*p-aknBCDE2F* and pSET-*kasOp*-aknBCDE2F* in *S. coelicolor* M1152 and M1152Δ*matAB*. (C) Production titers of UWM7 resulting from the engineering of pSET-*ermE*p-dpsABCDG* and pSET-*kasOp*-dpsABCDG* in *S. coelicolor* M1152 and M1152Δ*matAB*. (D) Production titers of SEK15 and WJ85 resulting from the engineering of pSET-*ermE*p-oxyABCD* and pSET-*kasOp*-oxyABCD* in *S. coelicolor* M1152 and M1152Δ*matAB*. ANOVA was carried out to determine the statistical significance between strains. The statistically significant comparisons are reflected with asterisks. The statistical significance of observed results was established with a $p < 0.05$. * indicates $p \leq 0.05$, ** indicates $p \leq 0.01$, *** indicates $p \leq 0.001$, and **** indicates $p \leq 0.0001$.

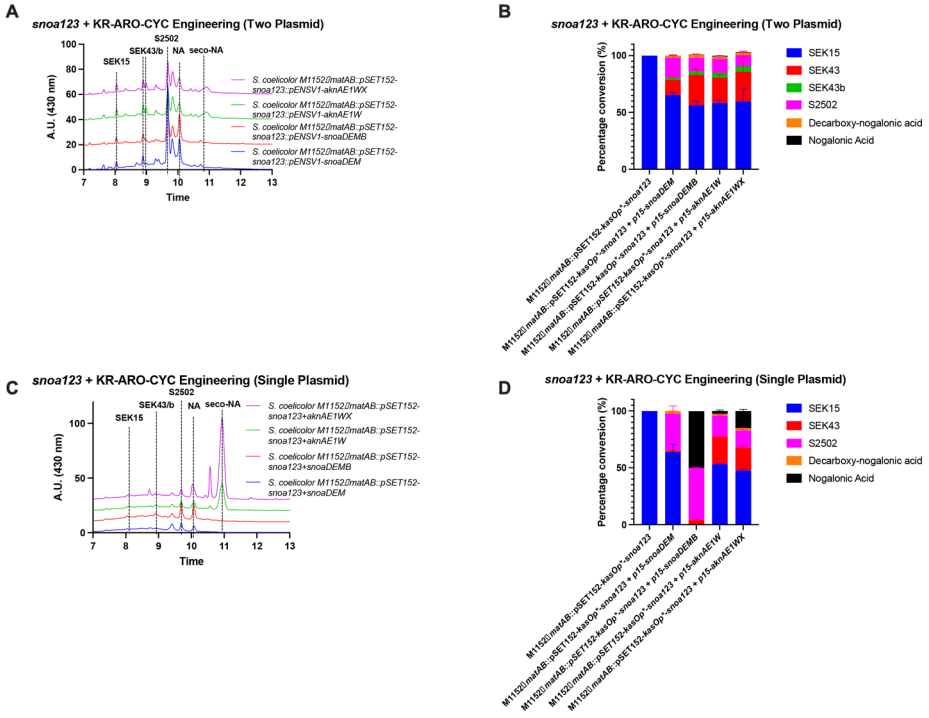

Figure 5. Engineering of KR/ARO/CYC cassettes with the *snoa123* minPKS. (A) Chromatograms of metabolites from two-plasmid *snoa123* and KR/ARO/CYC heterologous expression experiments. (B) Disposition of metabolites from two-plasmid *snoa123* and KR/ARO/CYC heterologous expression experiments. (C) Chromatograms of metabolites from one-plasmid *snoa123* and KR/ARO/CYC heterologous expression experiments. (D) Disposition of metabolites from one-plasmid *snoa123* and KR/ARO/CYC heterologous expression experiments.

Engineering of the *aknBCDE2F* and *dpsABCDG* operons in *S. coelicolor* M1152Δ*matAB* and *S. coelicolor* M1152 resulted in the expected production of UWM7 as the major metabolite at production titers of 1−7.5 mg/L in SG shake flask experiments (Figure 4). UWM7 exhibited a retention time of 8.42 min with a UV maximum of 290 nm and the expected mass in ESI+ mode $[M + H]^+ = 399$ m/z, as previously described (Supporting Information, Figure S13).[38] In each case, the corresponding *S. coelicolor* M1152Δ*matAB* resulted in a statistically significant increase in UWM7 production titers as compared to *S. coelicolor*

https://doi.org/10.1021/acssynbio.2c00498
ACS Synth. Biol. 2022, 11, 4193−4209

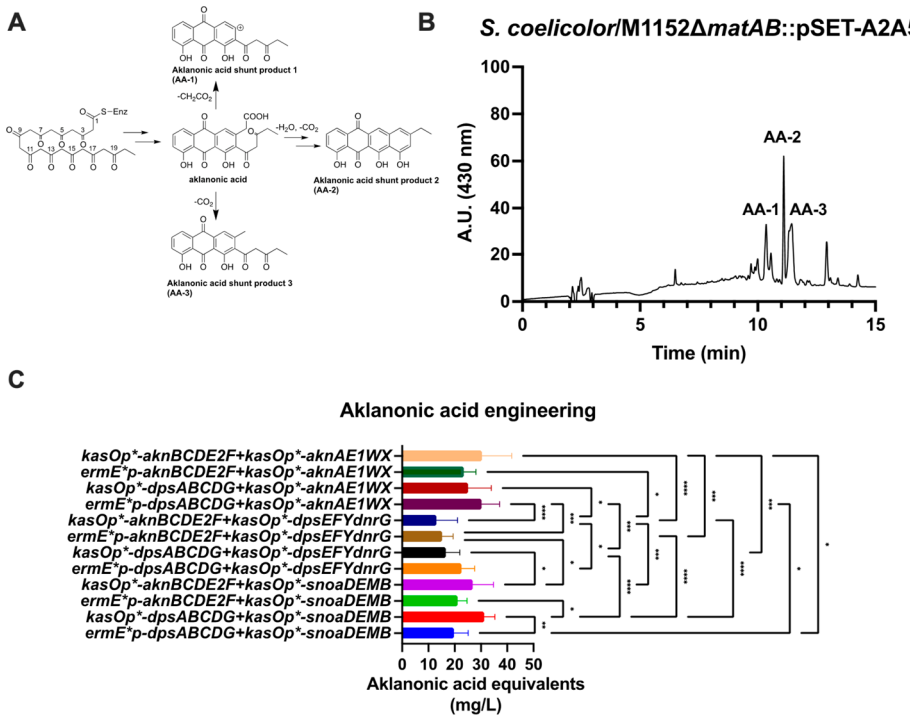

Figure 6. Engineering of aklanonic acid via combinatorial biosynthesis. (A) Scheme depicting degradation of aklanonic acid to its three detected shunt products (AA-1, AA-2, and AA-3). (B) Chromatogram of aklanonic acid degradation metabolites produced by a representative strain. (C) Aklanonic acid production titers resulting from full-factorial combinatorial biosynthesis of minPKS and KR/ARO/CYC/OXY genes. Error bars depict standard deviation. ANOVA was carried out to determine the statistical significance between strains. The statistically significant comparisons are reflected with asterisks. The statistical significance of observed results was established with a $p < 0.05$. * indicates $p \leq 0.05$, ** indicates $p \leq 0.01$, *** indicates $p \leq 0.001$, and **** indicates $p \leq 0.0001$.

M1152 ($p \leq 0.01$), and the *aknBCDE2F* operon was twice as productive as the *dpsABCDG* operon. The best construct featured the *kasOp** promoter fused to the *aknBCDE2F* operon (7.5 mg/L UWM7), which resulted in 33% greater UWM7 as compared to the *ermE*p* promoter fused to the *aknBCDE2F* operon ($p \leq 0.05$) (Figure 4).

Engineering of *oxyABCD* into the host strains resulted in the production of WJ85 as determined via HPLC-MS analysis (Supporting Information, Figure S14). WJ85 exhibited a retention time of 9.54 min with a UV maximum at 290 nm, and it exhibited a parental mass of $[M + H]^+ = 368$ m/z, as previously described.[37] The *ermE*p-oxyABCD* construct resulted in the production of 2.3 mg/L WJ85 in *S. coelicolor* M1152Δ*matAB*, as compared to the *kasOp*-oxyABCD* construct, which resulted in the production of 2.0 mg/L WJ85, although the difference between these two promoters was not statistically significant in this case (Figure 4). Due to the deletion of the Δ*matAB* operon, the *S. coelicolor* M1152Δ*matAB* strain accumulated 1 mg/L SEK15, which was not detected in *S. coelicolor* M1152. This result was interpreted to mean that *S. coelicolor* M1152Δ*matAB* strain exhibited improved production characteristics for minimal aromatic polyketides. The differences in production titer of WJ85 and SEK15 between M1152 and M1152Δ*matAB* were determined to be statistically significant based on ANOVA statistical analysis (Figure 4). Due to the low production yields of the *oxyABCD* operon, we did not pursue its use any further. In summation, we chose *S. coelicolor* M1152Δ*matAB* for further experiments to build out anthracyclinone pathways.

Engineering of Ketoreductases, Aromatases, and Cyclases. We next engineered reducing ketoreductase (KR), aromatase (ARO), and cyclase (CYC) gene cassettes into *S. coelicolor* M1152Δ*matAB* to generate tricyclic anthracyclinones (Figure 5). Starting from the enzyme-tethered poly-*β*-ketothioester synthesized by Snoa123, the 3-oxoacyl-[acyl carrier protein] ketoreductase (SnoaD/AknA) reduces the poly-*β*-ketothioester at 9-position, followed by C7−C12 first ring cyclization and aromatization (SnoaE/AknE1), C5−C14 s ring cyclization and C3−C16 third ring cyclization by the second-third ring cyclase (SnoaM/AknW), and C-12 oxidation by the anthrone oxygenase (SnoaB/AknX) (Figure 1). Genetic cassettes for *aknAE1W*, *aknAE1WX*, *snoaDEM*, and *snoaDEMB* were codon-optimized and cloned as described above under the control of the strong *p15* promoter from *Streptomyces albus* and cloned into a separate integrating vector pENSV1 for two plasmid coexpression or spliced into the pSET152BB-*kasOp*-snoa123* construct for expression of the entire cassette on a single plasmid.[24,44] Heterologous expression of *snoa123+snoaDEM*, *snoa123+snoaDEMB*, *snoa123+aknAE1W*, and *snoa123+aknAE1WX* on two plasmids resulted in the production of SEK15, and C7−C12 cyclized metabolites SEK43 and SEK43b, C7−C12 and C9−C14 cyclized metabolite S2502, and tricyclic anthracyclinones nogalonic acid and its rearrangement product decarboxy-nogalonic acid, as expected (Figure 5, Supporting Information, Figure S10). These metabolites were confirmed based on a comparison to authenticated biosynthetic standards from *S. lividans* TK24/pSY21c.[11] Percent conversion was calculated based on the integration of the peak areas at λ = 290 nm since the polyketides exhibit similar molar absorptivity coefficients at this wavelength (Figure 5).[11] This finding supports the role of AknA as a ketoreductase, AknE1 as an ARO/CYC, AknW as a second and third-ring cyclase, and AknX

https://doi.org/10.1021/acssynbio.2c00498
ACS Synth. Biol. 2022, 11, 4193−4209

as an anthrone oxygenase. Previously, Chung et al. demonstrated that the AknX anthrone oxygenase enhances the oxidation of emodin anthrone to emodin anthraquinone, although C-12 oxidation can also occur spontaneously.[10] Expression of the C-12 anthraquinol oxidase increased the formation of correctly cyclized tricyclic anthracyclinone intermediate, which confirms its essential role in the oxidation of nogalonic acid. Coexpression of the *snoa123* minPKS genes with the KR/ARO/CYC cassettes on one plasmid resulted in higher metabolic flux toward nogalonic acid (Figure 5). One possible explanation for this was offered by Yang et al., who observed that expression of type II PKS genes on the same plasmid in *E. coli* resulted in higher production of carminic acid.[45] Yang et al. postulated that colocalization of the minPKS genes and cyclase genes enhances the formation of the transient polyketide synthase complex, enhancing the production titer. Interestingly, the coexpression of *snoa123+aknAE1WX* on the same plasmid construct resulted in approximately 15% conversion to nogalonic acid. Expression of the *snoa123+snoaDEMB* construct resulted in a 50% conversion to nogalonic acid (Figure 5). These results demonstrate that the systematic testing of different orthologous gene combinations can provide additional insight into the compatibility of heterologous polyketide synthase components from related pathways. In addition, this approach can be used to provide biochemical evidence for gene products from uncharacterized pathways or for which only bioinformatic description is provided (e.g., AknA, AknE1, AknW).

We next decided to test the potential of BIOPOLYMER for combinatorial biosynthesis by carrying out a full factorial experiment for the biosynthesis of aklanonic acid. We designed this experiment by cloning combinations of the *aknBCDE2F* and *dpsABCDG* minPKS operons with the *aknAE1WX*, *snoaDEMB*, and *dpsEFY+dnrG* KR/ARO/CYC/OXY operons. The KR/ARO/CYC/OXY operons were all cloned under the control of the strong *kasOp** promoter since the strong transcriptional regulation of tailoring genes correlates with improved cyclic product formation and diminished shunt product accumulation in the actinorhodin pathway.[46] Expression of *aknBCDE2F* and *dpsABCDG* with KR/ARO/CYC/OXY genes resulted in the accumulation of three aklanonic acid-derived shunt products (AA-1, AA-2, and AA3), as previously described (Figure 6).[4] Mass spectroscopy confirmed the production of the three degradation products: AA-1, $[M - H]^-$ = 337 *m*/*z*; AA-2, $[M - H]^-$ = 333 *m*/*z*; AA-3, $[M - H]^-$ = 351 *m*/*z* (Supporting Information, Figure S85). All combinations assessed resulted in the production of aklanonic acid, which indicates that there is a significant biosynthetic collaboration between minPKS enzymes and ketoreductase/cyclase enzymes between the nogalamycin, daunorubicin, and aclacinomycin biosynthetic pathways (Figure 6). The production titers of aklanonic acid varied between 20 mg/L to 35 mg/L with the best combinations consisting of recombinant PKS systems *dpsABCDG+snoaDEMB* and *dpsABCDG+aknAE1WX* and the native *aknBCDE2F +aknAE1WX* pathway (Figure 6). We performed an analysis of variance (ANOVA) of all 12 strains to determine if the differences in production titer between the different strains were statistically significant (Figure 6). The ANOVA indicated that the observed results between many of the comparisons were statistically significant, which provides good evidence that the combinatorial biosynthesis of the minPKS and cyclase gene cassettes was responsible for the observed differences in production titer.

Engineering of Nogalamycinone and Structural Characterization of Anthracyclinones. We next decided to complete the aglycone engineering pathway by introducing the nogalonic acid methyltransferase, fourth-ring cyclase, and 7-ketoreductase from the nogalamycin biosynthetic pathway (Figure 1). The resulting construct, pSET152BB-*ermE*p-snoa123+kasOp*-aknAE1WX+sp44-snoaLCF* was transformed into *S. coelicolor* M1152Δ*matAB* and assessed for production of nogalamycinone. The order of genes in the *snoaLCF* operon was determined to be important for the complete conversion of nogalonic acid to nogalamycinone. Initially, cloning of the *snoaC* before *snoaL* and subsequent expression of the resulting plasmid yielded incomplete conversion from nogalonic acid to nogalamycinone. The resulting strains produced six compounds that could be detected via HPLC-MS, including nogalamycinone (**1**) which could be confirmed via comparison to an authentic HPLC standard (Figure S18). Interestingly, a new early eluting product was also detected that corresponded to a glucosylated derivative of nogalamycinone, as determined by mass spectrometric analysis in ESI− mode ($[M - H]^-$ = 559 *m*/*z*). The resulting strain was scaled up in a 5 L SG shake flask fermentation, extracted with 3 × 5 L of ethyl acetate, and fractionated via SiO_2 column chromatography in chloroform:-methanol systems on a Teledyne Combiflash 100 auto purification system. A second 2 L fermentation of the strain was carried out to isolate the unknown glucosylated nogalamycinone derivative. Compounds **1**−**6** were purified from additional prep-HPLC experiments.

The physicochemical properties of compounds **1**−**6** have been summarized in the experimental section (Supporting Information, Figures S16−S82, Tables S3 and S4). The chemical structures of the known anthracyclines nogalamycinone (**1**), auramycinone (**2**), 7-deoxy-nogalamycinone (**3**), and 7-deoxyauramycinone (**4**) were established by ^{1}H NMR, ^{13}C NMR, ^{1}H,^{1}H-COSY, ^{1}H,^{13}C-HMBC, and ^{1}H,^{1}H-NOESY NMR spectroscopic measurements (Supporting Information, Tables S3 and S4, Figures S16 and S17). Unexpectedly, both nogalamycinone and auramycinone were produced, which result from fourth ring cyclization reactions that generate the 9(*S*) and 9(*R*) products.[13,47] Compounds **1** and **2** were produced in an approximately 2:1 ratio, as were their shunt products **3** and **4**, which indicates that nogalamycinone and 7-deoxynogalamycinone were the preferred enzymatic products in the strain.

It is generally accepted that the codon-optimization of genes is known to improve translational efficiency by substituting rare codons in an mRNA sequence for preferred codons with abundant tRNAs, which leads to an increase in the concentration of the protein.[48] What is less understood is whether codon-optimization disrupts information that is present in wild-type mRNAs (e.g., rare codons that slow down the translation or that influence translation via binding to rRNA), which could impact protein conformation and function.[49] Hu et al. verified 342 synonymous codon variants of the scFv antibody and observed widely varying production titers, solubility, and binding affinity (e.g., ranging from no binding affinity to 10^{-8} M), while all proteins encoded the same original amino acid sequence.[50] Sander et al. demonstrated that synonymous codon changes in a fluorescent protein impacted the fluorescence and can alter the folded structure due to differences in the rate of translation and folding of the *N*- and *C*-termini.[51] It could be hypothesized that the production of **3** and **4** by codon optimized SnoaL could be due to protein conformational differences from

https://doi.org/10.1021/acssynbio.2c00498
ACS Synth. Biol. 2022, 11, 4193−4209

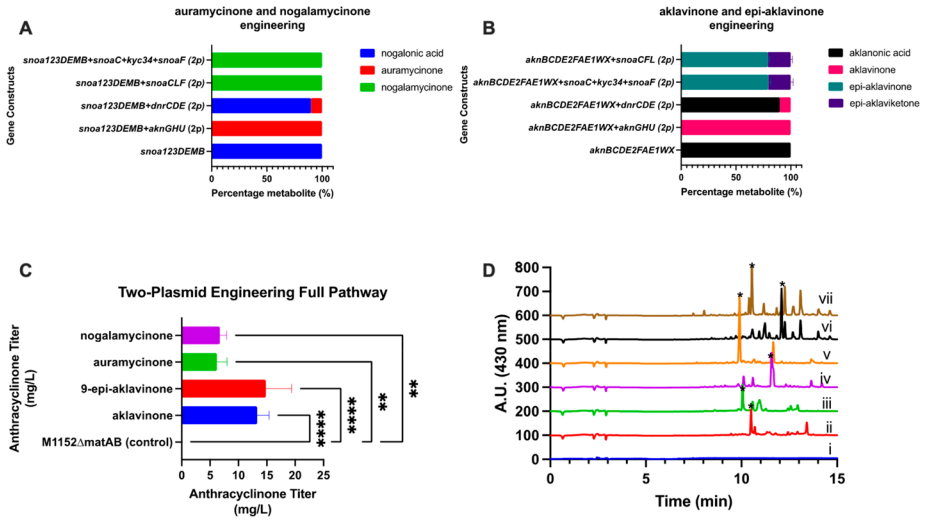

Figure 7. Full pathway engineering of anthracyclinone polyketide synthases. Engineering of methyltransferase, fourth-ring cyclase, and ketoreductase genes furnished anthracyclinone pathways in *S. coelicolor* M1152Δ*matAB*. (A) *S. coelicolor* M1152Δ*matAB*::pS2S5 was complemented with different constructs to biosynthesize different amounts of **1** and **2**. (B) *S. coelicolor* M1152Δ*matAB*::pA2A5 was complemented with different constructs to biosynthesize different amounts of **7** and **8**. (C) Production titer of anthracyclinones in strains expressing the entire pathway on two plasmids. Strains were grown in SG-TES liquid media for 5 days. Error bars reflect the SD of six replicates. Experimental groups were compared using a one-way ANOVA test to determine statistical significance. The statistical significance of observed results was established with a $p < 0.05$. * indicates $p \leq 0.05$, ** indicates $p \leq 0.01$, *** indicates $p \leq 0.001$, and **** indicates $p \leq 0.0001$. (D) HPLC chromatogram traces of different strains at 430 nm with major metabolites highlighted with an asterisk (*): (i) *S. coelicolor* M1152Δ*matAB*::pSET152; (ii) *S. coelicolor* M1152Δ*matAB*::A2A5 (aklanonic acid); (iii) *S. coelicolor* M1152Δ*matAB*::S2S5 (nogalonic acid); (iv) *S. coelicolor* M1152Δ*matAB*::S2S5A6 (auramycinone); (v) *S. coelicolor* M1152Δ*matAB*::S2S5S6 (nogalamycinone); (vi) *S. coelicolor* M1152Δ*matAB*::A2A5A6 (aklavinone); (vii) *S. coelicolor* M1152Δ*matAB*::A2A5S6 (9-*epi*-aklavinone).

the wild-type SnoaL which impact the binding of NAME in the active site, but this must be examined further.

The formation of **3**, **4**, and **5** requires the elimination of the 7-hydroxyl group, possibly due to the presence of a promiscuous CytA-like enzyme that is present in *S. coelicolor*. Gui et al. have characterized CytA as a promiscuous anthracycline-inactivating enzyme that reduces the C-7 position for a broad variety of anthracyclines in the cytorhodin pathway according to an NADH-dependent mechanism.[52]

Compound **5** was obtained as a yellow solid and displayed UV−vis characteristics like metabolites **1**−**4**. The molecular formula of **5** was established as $C_{21}H_{20}O_7$ based on (+)- and (−)-HRESIMS indicative of two additional protons as compared to compounds **3** and **4** (Supporting Information, Figure S64 and S65). Comparison of the ^{1}H and ^{13}C NMR of **5** and **3**/**4** (Supporting Information, Tables S3 and S4) revealed **5** to lack the C-9/C-10 bond connection and the methine proton signal at C-10 position (CH-10) in compounds **3**−**4** was replaced by CH_2 at δ_H 3.83 (CH_2-10). In addition, an additional oxygenated methine signal was observed at δ_H 3.80 (m, CH-9) in compound **5**. Furthermore, the singlet methyl signals in compounds **3**/**4** were replaced by a doublet methyl signal in **5** at δ_H 1.22 (d, 6.2). This was consistent with the presence of ^{1}H−^{1}H COSY correlations CH_3-13/H-9, H-9/CH_2-8, CH_2-8/CH_2-7 for **5** (Supporting Information, Figure S16). All the remaining 2D-NMR (^{1}H,^{1}H-COSY, HMBC, and NOESY) correlations are in full agreement with structure **5** (Supporting Information, Figures S63−S72). Based on the cumulative spectroscopic data, **5** differed solely from those of compounds **3**-**4** via their C-9/C-10 bond connection. Consistent with the cumulative 1D and 2D NMR data analysis, structure **5** was established as depicted in Figure 1 and named 9,10-*seco*-7-deoxy-nogalamycinone (**5**).

Compound **6** was isolated as a yellow solid and displayed UV−vis characteristics like anthracyclinones **1**−**4**. The molecular formula of **6** was established as $C_{27}H_{28}O_{13}$ based on (+) and (−)-HRESIMS, with $\Delta m/z$ = 162 higher than those of **1**, indicative of the presence of an extra hexose moiety in **6** (Supporting Information, Figures S74 and S75). Based on the ^{1}H NMR, ^{13}C NMR, NOESY, and ^{1}H,^{1}H-COSY data, the carbohydrate was unambiguously assigned as D-glucose (Supporting Information, Table S5 and Figure S17). Compared to **1**, the ^{13}C/^{1}H/HSQC NMR of **6** (Supporting Information, Table S1−S3) highlighted the presence of additional signals for the *O*-glycoside moiety in compound **6**. Based on the ^{1}H NMR, ^{13}C NMR, NOESY, and ^{1}H,^{1}H-COSY data, the carbohydrate was unambiguously assigned as D-glucose (Supporting Information, Table S5, Figure S17 and Figures S76−S82). The connection of the sugar moiety at the 4-position was established based on the observed critical HMBC correlation from H-1′ (δ_H 5.12, d, J = 7.7 Hz) to C-4 (δ_C 160.2). All the remaining 2D-NMR (^{1}H,^{1}H-COSY, HMBC, and NOESY) correlations are in full agreement with structure **6** (Supporting Information, Figure S17 and Figures S76−S82). As a new natural product and closely related to **1**, compound **6** was designated as 4-*β*-D-glucosyl-nogalamycinone (**6**).

Full Pathway Engineering of Anthracyclinones. We decided to complete the pathway engineering of other anthracyclinones, including auramycinone (**2**), aklavinone (**7**), and 9-*epi*-aklavinone (**8**). Fujiwara et al. isolated auramycinone as a C-20 anthracyclinone from *S. galilaeus* OBB-111, and aklavinone is a C-21 anthracyclinone that serves as the backbone for doxorubicin and aclacinomycin A.[53,54] 9-*epi*-Aklavinone was reported as a hybrid anthracyclinone resulting from the heterologous expression of *snoaL* from the nogalamycin biosynthetic pathway in a mutant strain of *S. peucetius* M18.[5]

https://doi.org/10.1021/acssynbio.2c00498
ACS Synth. Biol. 2022, 11, 4193−4209

Using the strains *S. coelicolor* M1152Δ*matAB*::pS2S5 (nogalonic acid producer) and *S. coelicolor* M1152Δ*matAB*::pA2A5 (aklanonic acid producer) as hosts, we cloned different combinations of *O*-methyltransferase genes (*aknG*, *dnrC*, *snoaC*), fourth-ring cyclases (*dnrD*, *kyc34*, *aknH*), and 7-ketoreductases (*snoaF*, *dnrE*, *aknU*) under the control of the strong *sp44* promoter and cloned them into the TG1-actinophage integrating vector pENTG1.[24] In brief, pENTG1 is a vector that encodes *bla* and *vph* for ampicillin and viomycin selection, respectively, and a codon-optimized version of the TG1 integrase and corresponding *attP* site for integration into the *S. coelicolor* TG1 *attB* chromosomal locus at a single copy.[55,56] The resulting vectors were expected to result in production of 9(*S*)-configured anthracyclinones (e.g., pENTG1-*sp44-snoaC+kyc34+snoaF*, pENTG1-*sp44-snoCLF*) or 9(*R*)-configured anthracyclinones (e.g., pENTG1-*sp44-dnrCDE* and pENTG1-*sp44-aknGHU*). Coexpression of these vectors in either of the two strains resulted in the production of the expected anthracyclinones (Figure 7). To produce nogalamycinone, *snoaLCF* and *snoaC+kyc34+snoaF* both resulted in the complete conversion of nogalonic acid. This result also provides experimental proof that *kyc34* from the keyicin biosynthetic pathway encodes a NAME cyclase, like *snoaL*.[57] Similarly, coexpression of *aknGHU* in *S. coelicolor* M1152Δ*matAB*::pS2S5 resulted in the complete conversion of nogalonic acid to **2**. For the production of **7**, when *S. coelicolor* M1152Δ*matAB*::pA2A5 was complemented with *aknGHU*, complete conversion of aklanonic acid was observed. Lastly, the complementation of the aklanonic acid producer with either *snoaLCF* or *snoaC+kyc34+snoaF* resulted in approximately 80% conversion to 9-*epi*-aklavinone. This experiment demonstrates that the BIOPOLYMER system can be used to produce all the naturally occurring reduced anthracyclinone analogues.

Next, we cloned the aklavinone, 9-*epi*-aklavinone, auramycinone, and nogalamycinone pathways onto a single integrating plasmid. To accomplish this, a new version of pSET152 was cloned in which the strong synthetic *tt-sbi-A* transcriptional terminator from *Mycobacterium tuberculosis* and the strong *fd* phage terminator were inserted 5′ and 3′ of the BioBricks cloning sites,[58−60] which was designated as pSET154BB (Supporting Information, Table S1). The resulting plasmids encoding aklavinone (e.g., pSET154BB-*kasOp*-aknBCDE2F+kasOp*-aknAE1WX+sp44-aknGHU*), auramycinone (pSET154BB-*kasOp*-snoa123+kasOp*-snoaDEMB+sp44-aknGHU*), and nogalamycinone (pSET154BB-*kasOp*-snoa123+kasOp*-snoaDEMB+sp44-snoaC+kyc34+snoaF*) were transformed into *S. coelicolor* M1152Δ*matAB* to quantify the production titers of the intended anthracyclinones. In addition, we also transformed in the nogalamycinone pathway plasmid pSET152BB-*kasOp*-snoa123+kasOp*-aknAE1WX + sp44-snoaCLF*, which was used to isolate compounds **1**−**6** for structure elucidation. The strains were fermented in SG-TES media and E1 media, which are two media used in our laboratories to produce polyketides. In the case of the first four plasmids for aklavinone, 9-*epi*-aklavinone, auramycinone, and nogalamycinone, the yields of anthracyclinones were lower than those obtained with the two-plasmid expression system (Figure 8). *S. coelicolor* M1152Δ*matAB* harboring these constructs produced a mean production titer of 2.22 mg/L aklavinone in SG-TES media and 0.67 mg/L in E1 media, 1.35 mg/L 9-*epi*-aklavinone in SG-TES media and 0.98 mg/L 9-*epi*-aklavinone in E1 media, 0.94 mg/L auramycinone in SG-TES media and 0.39 mg/L auramycinone in E1 media, and 3.22 mg/L nogalamycinone in SG-TES media and 1.32 mg/L nogalamycinone in E1 media. In contrast, the fully codon-optimized construct pSET152BB-*kasOp*-snoa123+kasOp*-aknAE1WX+sp44-snoaCLF* resulted in the production of approximately 33-fold higher levels of nogalamycinone at 103 mg/L in SG-TES media and 45 mg/L in E1 media E1 media. The yields of anthracyclinones indicate that the metabolic flux is controlled by the expression of the minimal polyketide synthase. This is especially highlighted by the greatly increased production titer of nogalamycinone resulting from the fully codon-optimized nogalamycinone construct, which could be explained by the enhanced translation of the Snoa123 minPKS complex. This result indicates that additional optimization of the *aknBCDE2F* minPKS cassette is still required. Several strategies could be pursued, including codon-optimization, additional promoter

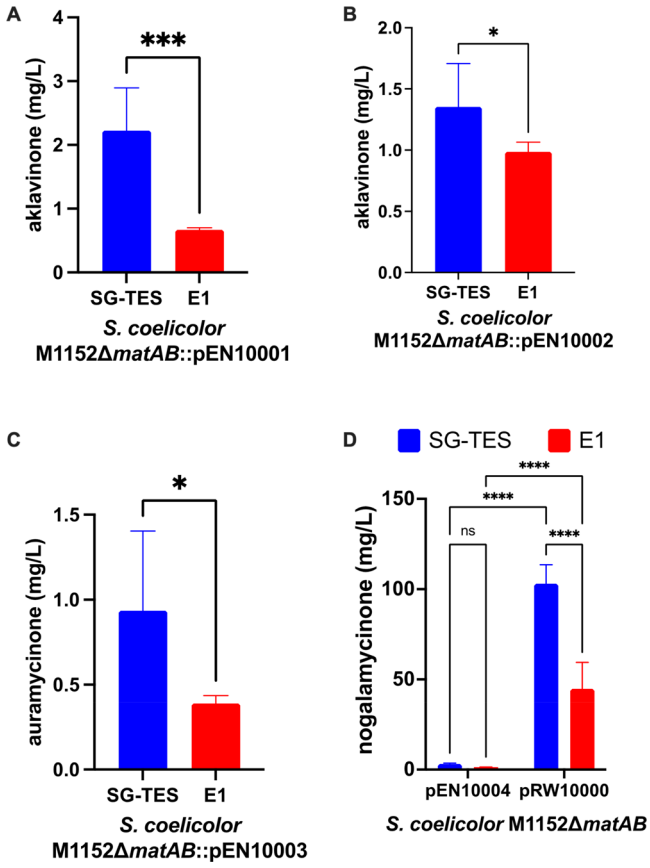

Figure 8. Production titers resulting from the expression of anthracyclinone pathways on a single plasmid. *S. coelicolor* M1152Δ*matAB* was transformed with vectors (A) pSET154BB-*kasOp*-aknBCDE2F+kasOp*-aknAE1WX+sp44-aknGHU* (pEN10001, aklavinone pathway), (B) pSET154BB-*kasOp*-aknBCDE2F+kasOp*-aknAE1WX+sp44-snoaC+kyc34+snoaF* (pEN10002, 9-*epi*-aklavinone pathway), (C) pSET154BB-*kasOp*-snoa123+kasOp*-snoaDEMB+sp44-aknGHU* (pEN10003, auramycinone pathway), or (D) pSET154BB-*kasOp*-snoa123+kasOp*-snoaDEMB+sp44-snoaC+kyc34+snoaF* (pEN10004, wild-type nogalamycinone pathway) or pSET152BB-*kasOp*-snoa123+kasOp*-aknAE1WX + sp44-snoaCLF* (pRW10000, codon-optimized nogalamycinone pathway) and grown in shake flasks of SG-TES or E1 liquid media for 5 days. Error bars reflect the standard deviation of six replicates. Post hoc Student's *t* tests were performed to determine statistical significance. The statistical significance of observed results was established with a $p < 0.05$. * indicates $p \leq 0.05$, ** indicates $p \leq 0.01$, *** indicates $p \leq 0.001$, and **** indicates $p \leq 0.0001$.

https://doi.org/10.1021/acssynbio.2c00498
ACS Synth. Biol. 2022, 11, 4193−4209

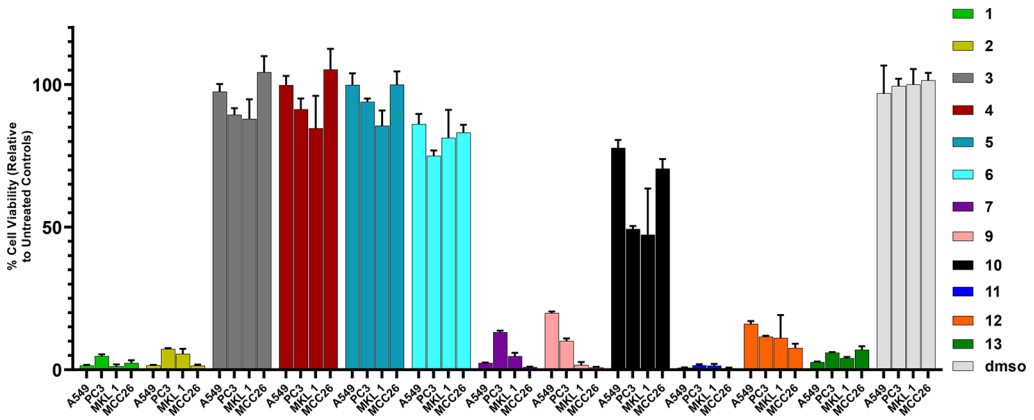

Figure 9. % Viability of A549 (non-small-cell lung) and PC3 (prostate) human cancer cell lines, and Merkel cells (MKL1 and MCC26) (after 72 h) at 80 μM concentration of compounds **1**−**7** and **9**−**13**.

Table 3. Cytotoxic Activities of Compounds 1−13[a]

compounds	IC_{50} μM		IC_{50} μM	
	A549	PC3	MKL1	MCC26
Nogalamycinone (**1**)	30.30 ± 2.30	18.60 ± 3.61	29.30 ± 10.30	36.50 ± 5.34
Auramycinone (**2**)	31.00 ± 0.96	13.90 ± 3.66	26.10 ± 1.16	30.40 ± 2.01
7-Deoxy-nogalamycinone (**3**)	>80	>80	>80	>80
7-Deoxyauramycinone (**4**)	>80	>80	>80	>80
9,10-*seco*-7-Deoxy-nogalamycinone (**5**)	>80	>80	>80	>80
4-β-D-Glucosyl-nogalamycinone (**6**)	>80	>80	>80	>80
Aklavinone (**7**)	17.80 ± 6.24	7.72 ± 0.57	22.70 ± 1.79	26.10 ± 0.66
Nogalamycin A (**9**)	0.056 ± 0.011	0.021 ± 0.002*	0.062 ± 0.035*	0.095 ± 0.044*
Nogalamycin KO (**10**)	>80	>80	>80	>80
Nogalamycin R (**11**)	32.30 ± 4.09	28.30 ± 3.10	18.50 ± 2.64	35.60 ± 2.73
3′,4′-Demethoxy-nogalose-1-hydroxy-nogalamycinone (**12**)	2.88 ± 0.23	2.88 ± 0.79	1.07 ± 0.011	3.50 ± 0.36
Aclacinomycin T (**13**)	3.62 ± 0.087	2.00 ± 0.15	2.35 ± 0.78	10.70 ± 4.32

[a]Cytotoxicity IC_{50} values were obtained after 72 h incubation. Actinomycin D and H_2O_2 [A549 (non-small-cell lung), PC3 (prostate) human cancer cell lines, and Merkel cells MKL1 and MCC26] were used as a positive control at 20 μM and 1 mM concentration, respectively (0% viable cells, n = 3, but *(n = 6)).

engineering, multiplexed site-specific genome engineering (MSGE) to increase the number of ϕC31 *attB* sites in the chromosome, and even engineering of the endogenous housekeeping sigma factor σ^{hrdB} to establish a self-sustaining production system (*StSS*).[61−63] As determined by Student's *t*-test, SG-TES media was better than E1 media to produce all four anthracyclinones in this strain ($p \leq 0.05$).

Human Cancer Cell Viability Assays. Next, we assessed the antiproliferative activity of anthracyclinones **1**−**7** and compared the activity to anthracycline compounds previously isolated in our lab: nogalamycin A (**9**), nogalamycin KO (**10**), nogalamycin R (**11**), 3′,4′-demethoxy-nogalose-1-hydroxy-nogalamycinone (**12**), and aclacinomycin T (**13**).[33,64,65] First, the compounds were assessed in a single dose (80 μM) viability assay against a representative set of human cancer cell lines [A549 (non-small-cell lung epithelial carcinoma), PC3 (prostate adenocarcinoma), and MKL1 (polyomavirus-positive Merkel carcinoma) and MCC26 (virus-negative Merkel carcinoma) (Figure 9)]. The most active compounds were anthracyclines nogalamycin A (**9**), nogalamycin R (**11**), 3′,4′-demethoxy-nogalose-1-hydroxy-nogalamycinone (**12**), and aclacinomycin T (**13**). This result was expected since the glycoside moiety of the anthracyclines is essential for binding to DNA and inhibition of DNA topoisomerases.[66] Compounds **6** and **10** exhibited slight antiproliferative activity (**6**: 75−85% T/C; **10**: 50−75% T/C). In the single dose experiment **1**, **2**, and **7** exhibited antiproliferative activity (<10% T/C) comparable to previously reported compounds **9**, **11**, **12**, and **13**. Compounds **3**−**5** did not exhibit any activity in the assay.

The dose−response relationships of **1**, **2**, **6**, **7**, and **9**−**13** were established for A549 and PC3 cells and Merkel cells MKL1 and MCC26 (Supporting Information, Figure S83 and S84). The half-maximal inhibitory concentration values (IC_{50}) were determined for the entire cancer cell panel (Table 3). Previously reported compound **9** was the most cytotoxic among the set tested, with IC_{50} values ranging from 21 to 95 nM. In contrast, compound **7** was the most active among the analogues derived from the current study, with IC_{50} values ranging from 8 to 26 μM. This is consistent with previous studies highlighting the contribution of anthracycline glycosylation to potency, selectivity, and ADMET.[67]

CONCLUSIONS

The "mixing and matching" of PKS components for the reconstitution of non-native aromatic polyketide synthases has been the subject of numerous in vivo studies, which provided the foundational basis for the biosynthetic logic of these enzymes.[68−72] However, these experiments often utilized PKS enzymes from disparate pathways, which resulted in recombinant PKS systems that produced low yields of the expected novel

https://doi.org/10.1021/acssynbio.2c00498
ACS Synth. Biol. 2022, 11, 4193−4209

polyketides, or that failed.[73] This resulted in the observation that the failure of polyketide combinatorial biosynthesis derives from the inflexibility of downstream enzymes to recognize novel substrates or lack of enzyme solubility.[74] In contrast, focusing on enzymes from evolutionarily related pathways might provide more fertile ground for combinatorial biosynthesis efforts and improved substrate turnover to produce novel polyketides. More recently, the use of cell-free biosynthesis (also known as "combinatorial biosynthetic enzymology") has demonstrated the success of this "mix-and-match" approach via the use of PKS enzymes from closely related pathways for the synthesis of defucogilvocarcin M and steffimycinone *in vitro*.[75,76]

A "Design-Build-Test-Learn" (DBTL) approach has been suggested to uncover the logic of recombinant PKS systems.[77] This is the approach that we have currently undertaken with the development of the BIOPOLYMER toolbox, via the identification of PKS gene orthologs that interact positively and result in the production of expected polyketides in *S. coelicolor* M1152Δ*matAB*. In this work, the "design phase" resulted in the selection of different *S. coelicolor* hosts, strong promoters, vector combinations, and gene orthologs. The "build phase" was facilitated by the use of the BioBricks-[RFC 10] synthetic biology standard and straightforward transformation of *Streptomyces* spp. using intergeneric conjugation. The "test phase" carried out several different comparisons of anthracyclinone genes to identify those with the best conversion percentage and production yield of the expected polyketide. Lastly, the "learn phase" resulted in the identification of an optimal production host, *S. coelicolor* M1152Δ*matAB*, promoter and gene combinations, and the structure elucidation of several anthracyclinones (**1**−**4**) and new compounds 9,10-*seco*-7-deoxy-nogalamycinone (**5**) and 4-*O*-*β*-D-glucosyl-nogalamycinone (**6**). Furthermore, the production platform was used to generate newly engineered metabolites for testing in mammalian cancer cell viability assays. These assays confirmed that the 7-*O*-glycoside is important for the anticancer activity of anthracyclines, including nogalamycin A (**9**), 3′,4′-demethoxy-nogalose-1-hydroxy-nogalamycinone (**12**), and aclacinomycin T (**13**). Nevertheless, the observation that nogalamycinone, auramycinone, and aklavinone exhibited moderate cytotoxicity is encouraging for further efforts to generate diverse anthracycline analogues incorporating these pharmacophores.

The pathway engineering studies described here resulted in the unexpected generation of 7-deoxygenated metabolites, **3** and **4**, and two new anthracycline metabolites, 9,10-*seco*-7-deoxy-nogalamycinone (**5**) and 4-*O*-*β*-D-glucosyl-nogalamycinone (**6**). Despite being a genome minimalized "superhost", the genome *S. coelicolor* M1152Δ*matAB* still encodes hypothetical proteins that can interact with heterologous pathways in an unanticipated fashion. Compounds **3**, **4**, and **5** are thought to derive from the dehydration of the 7-hydroxyl group via an ancillary CytA-like enzyme.[52] CytA has been shown to catalyze the 7-reduction of a wide variety of anthracycline saccharide chains within the cytorhodin pathway. CytA could be part of a larger family of promiscuous enzymes encoded within actinomycete genomes, perhaps as an evolutionary self-defense strategy against xenobiotics. Studies are ongoing to identify this reductase within *S. coelicolor* M1152.

Compound **6** is thought to derive from a hypothetical glucosyltransferase that catalyzes the transfer of NDP-D-glucose to the 4-position of nogalamycinone. Studies are ongoing to identify the glucosyltransferase responsible for the transfer of NDP-D-glucose to nogalamycinone. The macrolide glucosyltransferase OleD has been mutagenized via directed evolution to afford one of the most substrate-promiscuous glycosyltransferase catalysts for the glycorandomization of a variety of diverse natural products.[78−81] Notably, **6** has a similar 4-*O*-glycosylation pattern to the previously discovered mutactimycin PR, andicoquinones A−D, komodoquinone A, and histomodulin.[82] In the cancer cell line cytotoxicity assays, the 4-*β*-D-glucose substitution was deleterious to the topoisomerase II inhibition of **6** since this compound was only slightly cytotoxic (Figure 9). Instead, the closely related 4-*O*-*β*-D-glucopyranuronosyl-*ε*-rhodomycinone (histomodulin) has been shown to exhibit upregulation of major histocompatibility class-I molecules on the surface of T-cells.[83] This class of 4-*O*-glucosides could be further investigated for unique immunomodulatory activities as potential new anticancer or anti-infective agents.

In summation, BIOPOLYMER is a flexible synthetic biology platform for the rational programming of *S. coelicolor* to produce aromatic polyketide natural products. We anticipate that BIOPOLYMER will be useful for providing access to known and new anthracycline natural products for antiproliferative activity studies. We also expect that BIOPOLYMER could be useful for studying cryptic type II PKS pathways and for providing a robust toolset for unraveling their biosynthetic logic.

METHODS

Bacterial Strains and Growth Conditions. *Escherichia coli* JM109 and *E. coli* ET12567 were grown in LB broth or LB agar at 37 °C as previously described.[84] *E. coli* JM109 was used for plasmid propagation and subcloning, while *E. coli* ET12567/pUZ8002 was used as the conjugation donor host for mobilizing expression vectors into *S. coelicolor* and *S. lividans* expression hosts as previously described.[85] When appropriate, ampicillin (100 μg mL^{-1}), kanamycin (25 μg mL^{-1}), apramycin (25 μg mL^{-1}), viomycin (25 μg mL^{-1}), and nalidixic acid (30 μg mL^{-1}) were supplemented to media to select for recombinant microorganisms.

S. lividans and *S. coelicolor* derivative strains were routinely maintained on Soya-Mannitol Flour (SFM) agar supplemented with 10 mM $MgCl_2$ and International Streptomyces Project medium #4 (ISP4) (BD Difco) at 30 °C as described previously.[85] *S. lividans* K4−114 was a gift from Prof. Dr. Lou Charkoudian (Haverford College, PA). *S. coelicolor* M1146 and *S. coelicolor* M1152 were gifts from Prof. Dr. Mervyn Bibb's laboratory (John Innes Centre, Norwich, UK). *S. coelicolor* M1152Δ*matAB* was generated via replacement of the *sco2963-sco2962 matAB* locus via PCR-ReDirect mutagenesis as previously described (Supporting Information, Method 1).[19] For liquid culturing, *S. coelicolor* derivative strains were grown in TSB media (3 mL) to ferment the seed culture and then grown in a modified 50 mL SG-TES liquid medium (soytone 10 g, glucose 20 g, yeast extract 5 g, TES free acid 5.73 g, $CoCl_2$ 1 mg, per liter) or 50 mL E1 medium for production for 7 days.[86] All media and reagents were purchased from Thermo-Fisher Scientific.

General Manipulations. Routine genetic cloning and plasmid manipulation were carried out in *E. coli* JM109 (New England Biolabs). *E. coli* ET12567/pUZ8002 was used as the host for intergeneric conjugation with *S. coelicolor* as previously described.[85] *E. coli* chemically competent cells were prepared using the Mix and Go! *E. coli* Transformation Kit (Zymo Research). *E. coli* was transformed with plasmid DNA via chemically competent heat-shock transformation as described previously. Plasmid DNA was isolated via the Wizard Plus SV

https://doi.org/10.1021/acssynbio.2c00498
ACS Synth. Biol. 2022, 11, 4193−4209

Minipreps DNA Purification System by following the manufacturer's protocols (Promega). All molecular biology reagents and enzymes used for plasmid construction were purchased from New England Biolabs. The conjugation donor host *E. coli* ET12567/pUZ8002 was transformed with constructs for mobilization into *S. coelicolor* strains, as previously described. For each transformation, 9−12 independent exconjugants were plated to DNA plates supplemented with antibiotics and grown for 4−5 days until the formation of vegetative mycelium.

General Experimental Procedures. Ultraviolet−visible (UV−vis) spectra were taken directly from analytical HPLC runs and show relative intensities. All NMR spectra were recorded at 600 MHz (14.1 T) using a Bruker Avance Neo console equipped with a TCI 5 mm cryoprobe (all spectra were processed in Bruker Topspin 4.1.3 version, and 2D spectra were apodized with QSINE or SINE window functions and zero-filled to 256 × 1024 points), and spectra were analyzed and plotted using Mnova [where δ-values were referenced to respective solvent signals (CD_3OD, δ_H 3.31 ppm, δ_C 49.15 ppm; $CDCl_3$, δ_H 7.24 ppm, δ_C 77.23 ppm)] (Bruker BioSpin Corporation, Billerica, MA). High-resolution electrospray ionization (HRESI) mass spectra were recorded on AB SCIEX Triple TOF 5600 system. HPLC-UV/MS analyses were accomplished with an Agilent InfinityLab LC/MSD mass spectrometer (MS Model G6125B; Agilent Technologies, Santa Clara, CA, USA) equipped with an Agilent 1260 Infinity II Series Quaternary LC system and a Phenomenex NX-C18 column (250 × 4.6 mm, 5 μm) [Method: solvent A: H_2O/0.1% formic acid, solvent B: CH_3CN; flow rate: 0.5 mL min^{-1}; 0−30 min, 5−100% B (linear gradient); 30−35 min, 100% B; 35−36 min, 100%−5% B; 36−40 min, 5% B]. HPLC-UV analyses were carried out in a Agilent 1260 system equipped with a photodiode array detector (PDA) and a Phenomenex C_{18} column (Phenomenex, Torrance, CA; 250 × 4.6 mm, 5 μm; solvent A: H_2O/0.1% TFA, solvent B: CH_3CN; flow rate: 1.0 mL min^{-1}; 0−30 min, 5−100% B; 30−35 min, 100% B; 35−36 min, 100%−5% B; 36−40 min, 5% B). Semipreparative HPLC were carried out in a Agilent 1260 Infinity II (Prep HPLC) system equipped with a Diode Array Detector (DAD) and a Gemini 5 μm C_{18} 110 Å, LC column 250 × 10 mm (Phenomenex, Torrance, CA) [**Method A:** H_2O/0.025% TFA; solvent B: CH_3CN; flow rate: 5.0 mL min^{-1}; 0−2 min, 15% B; 2−31 min, 15−100% B; 31−33 min, 100% B; 33−34 min, 100−15% B; 34−36 min, 10% B; **Method B:** solvent A: H_2O/0.025% TFA; solvent B: CH_3CN; flow rate: 5.0 mL min^{-1}; 0−2 min, 15% B; 2−28 min, 15−75% B; 28−30 min, 75−100% B; 30−32 min, 100% B; 32−34 min, 100−15% B; 34−36 min, 10% B; **Method C:** solvent A: H_2O/0.025% TFA; solvent B: CH_3CN; flow rate: 5.0 mL min^{-1}; 0−2 min, 25% B; 2−28 min, 25−85% B; 28−30 min, 85−100% B; 30−32 min, 100% B; 32−34 min, 100−25% B; 34−36 min, 25% B; **Method D:** solvent A: H_2O/0.025% TFA; solvent B: CH_3CN; flow rate: 5.0 mL min^{-1}; 0−2 min, 10% B; 2−22 min, 10−65% B; 22−25 min, 65−100% B; 25−27 min, 100% B; 27−28 min, 100−10% B; 28−30 min, 10% B]. All solvents used were of ACS grade and purchased from Pharmco-AAPER (Brookfield, CT). Size exclusion chromatography was performed on Sephadex LH-20 (25−100 μm; GE Healthcare, Piscataway, NJ). A549 and PC3 cells were obtained from ATCC (Manassas, VA). All other reagents used were reagent grade and purchased from Sigma-Aldrich (Saint Louis, MO).

Statistical Analyses. The statistical significance of the impact of genetic manipulations and combinatorially assessed variables on production was assessed via post hoc analysis. One-way ANOVA, two-way ANOVA, and Student's *t* test analyses were performed using GraphPad Prism version 9.4.1 for Mac OS X, GraphPad Software, San Diego, CA, USA, www.graphpad.com.

Cancer Cell Line Viability Assay. A549 and PC3 cells were obtained from ATCC (Manassas, VA). Merkel cells MKL1 and MCC26 were a gift from Dr. Isaac Brownell's laboratory (NIH/NIAMS, Bethesda, MD). All other reagents used were reagent grade and purchased from Sigma-Aldrich (Saint Louis, MO). Human cell line cytotoxicity [A549 (non-small-cell lung) and PC3 (prostate) human cancer cell lines, Merkel cells MKL1 and MCC26] assays were accomplished in triplicate following our previously reported protocols.[87−90] Vehicle (DMSO) was used as the negative control, and actinomycin D and H_2O_2 (A549 and PC3; MKL1 and MCC26) were used as positive control at 20 μM and 1 mM concentration, respectively.

Isolation of Compounds 1−6. *S. coelicolor* M1152Δ*matAB*::pRW10000 was grown on a soya mannitol flour (SFM) agar plate until well-sporulated for 4−5 days. Spores from the SFM agar plate were used to inoculate a seed culture of 50 mL tryptic soy broth in a 250 mL Erlenmeyer shake flask and were grown for 48 h in an orbital shaker at 30 °C at 220 rpm. One milliliter of seed culture was used to inoculate each of the 40 × 100 mL SG liquid media shake flasks (1% v/v inoculum) which were fermented for 5 days. The 4 L culture was extracted 4 × 4 L of ethyl acetate +0.1% formic acid and was dried in vacuo on a rotary evaporator. The resulting 2.3 g crude extract was dissolved in 9:1 chloroform−methanol and was loaded onto a 25 g SiO_2 solid load cartridge and chromatographed on a 24 g RediSep Gold Normal Phase Silica cartridge (Teledyne-ISCO). The extract was fractionated using the gradient setting and chloroform−methanol systems [**Method E:** chloroform; solvent B: methanol; flow rate: 40.0 mL min^{-1}; 0−15 min, 0−10% B.] Compounds **1**−**5** eluted in combined fraction at a retention time of 3.0 min. The compounds were individually resolved and purified via preparatory HPLC.

The same strain was separately grown in 2 L of E1 media to produce substantive amounts of compound 6. The 2 L fermentation was centrifuged to separate the cell pellet from the fermentation broth. The fermentation broth was extracted with 40 g Amberlite XAD-7 resin for 16 h, washed with 2 L of water, eluted with 1 L of methanol, and dried in vacuo on a rotary evaporator. Compound **6** was isolated via preparatory HPLC.

Physicochemical Properties of Compounds 1−6. *Nogalamycinone (**1**).* $C_{21}H_{18}O_8$ (398); yellow solid; *HPLC-*R_t = 22.72 min (Supporting Information, Figures S18 − S28); UV−vis λ_{max} 198, 228, 258, 290 (sh), 430 nm; ^1H NMR ($CDCl_3$, 600 MHz) and ^{13}C NMR ($CDCl_3$, 150 MHz), see Tables S3 and S4; (−)-ESI-MS: *m*/*z* 397 $[M - H]^-$; (+)-ESI-MS: *m*/*z* 381 $[(M\text{-}H_2O) + H]^+$, 363 $[(M\text{-}2H_2O) + H]^+$; (−)-HRESI-MS: *m*/*z* 397.0929 $[M - H]^-$ (calcd for $C_{21}H_{17}O_8$, 397.0929); (+)-HRESI-MS: *m*/*z* 363.0860 $[(M\text{-}2H_2O) + H]^+$ (calcd. for $C_{21}H_{15}O_6$, 363.0863), 421.0865 $[M + Na]^+$ (calcd for $C_{21}H_{18}O_8Na$, 421.0893), 819.1865 $[2\ M + Na]^+$ (calcd for $C_{42}H_{36}O_{16}Na$, 819.1895).

*Auramycinone (9-epi-Nogalamycinone) (**2**).* $C_{21}H_{18}O_8$ (398); yellow solid; *HPLC-*R_t = 22.68 min (Supporting Information, Figures S29 − S39); UV−vis λ_{max} 196, 228, 260, 290 (sh), 430 nm; ^1H NMR ($CDCl_3$, 600 MHz) and ^{13}C NMR ($CDCl_3$, 150 MHz), see Tables S3 and S4; (−)-ESI-MS: *m*/*z* 397 $[M - H]^-$; (+)-ESI-MS: *m*/*z* 381 $[(M\text{-}H_2O) + H]^+$, 363

https://doi.org/10.1021/acssynbio.2c00498
ACS Synth. Biol. 2022, 11, 4193−4209

[(M-2H_2O) + H]$^+$; (−)-HRESI-MS: m/z 397.0930 [M − H]$^-$ (calcd for $C_{21}H_{17}O_8$, 397.0929); (+)-HRESI-MS: m/z 363.0863 [(M-2H_2O) + H]$^+$ (calcd for $C_{21}H_{15}O_6$, 363.0863), 421.0890 [M + Na]$^+$ (calcd for $C_{21}H_{18}O_8Na$, 421.0893), 819.1913 [2 M + Na]$^+$ (calcd for $C_{42}H_{36}O_{16}Na$, 819.1895).

7-Deoxy-nogalamycinone (**3**). $C_{21}H_{18}O_7$ (382); yellow solid; *HPLC-*R_t = 28.35 min (Supporting Information, Figures S40 − S50); UV−vis λ_{max} 200, 228, 260, 290 (sh), 432 nm; ^{1}H NMR ($CDCl_3$, 600 MHz) and ^{13}C NMR ($CDCl_3$, 150 MHz), see Tables S3 and S4; (−)-ESI-MS: m/z 381 [M − H]$^-$; (+)-ESI-MS: m/z 383 [M + H]$^+$, 365 [(M-H_2O) + H]$^+$; (−)-HRESI-MS: m/z 381.0971 [M − H]$^-$ (calcd for $C_{21}H_{17}O_7$, 381.0979); (+)-HRESI-MS: m/z 365.1241 [(M-H_2O) + H]$^+$ (calcd for $C_{21}H_{17}O_6$, 365.1019), 383.1355 [M + H]$^+$ (calcd for $C_{21}H_{19}O_7$, 383.1126), 405.1187 [M + Na]$^+$ (calcd for $C_{21}H_{18}O_7Na$, 405.09447), 787.2493 [2 M + Na]$^+$ (calcd for $C_{42}H_{36}O_{14}Na$, 787.1997).

7-Deoxyauramycinone (9-epi-7-deoxy-nogalamycinone) (**4**). $C_{21}H_{18}O_7$ (382); yellow solid; *HPLC-*R_t = 28.02 min (Supporting Information, Figures S51 − S61); UV−vis λ_{max} 200, 228, 260, 290 (sh), 432 nm; ^{1}H NMR ($CDCl_3$, 600 MHz) and ^{13}C NMR ($CDCl_3$, 150 MHz), see Tables S3 and S4; (−)-ESI-MS: m/z 381 [M − H]$^-$; (+)-ESI-MS: m/z 405 [M + Na]$^+$, 383 [M + H]$^+$, 365 [(M-H_2O) + H]$^+$; (−)-HRESI-MS: m/z 381.0971 [M − H]$^-$ (calcd for $C_{21}H_{17}O_7$, 381.0979); (+)-HRESI-MS: m/z 383.1188 [M + H]$^+$ (calcd for $C_{21}H_{19}O_7$, 383.1126).

9,10-seco-7-Deoxy-nogalamycinone (**5**). $C_{21}H_{20}O_7$ (384); yellow solid; *HPLC-*R_t = 27.95 min (Supporting Information, Figures S62 − S72); UV−vis λ_{max} 200, 228, 260, 290 (sh), 434 nm; ^{1}H NMR ($CDCl_3$, 600 MHz) and ^{13}C NMR ($CDCl_3$, 150 MHz), see Tables S3 and S4; (−)-ESI-MS: m/z 383 [M − H]$^-$; (+)-ESI-MS: m/z 367 [(M-H_2O) + H]$^+$; (−)-HRESI-MS: m/z 383.1129 [M − H]$^-$ (calcd for $C_{21}H_{19}O_7$, 383.1136); (+)-HRESI-MS: m/z 367.1066 [(M-H_2O) + H]$^+$ (calcd for $C_{21}H_{19}O_6$, 367.1176), 407.0976 [M + Na]$^+$ (calcd for $C_{21}H_{20}O_7Na$, 407.1101), 791.2076 [2 M + Na]$^+$ (calcd for $C_{42}H_{40}O_{14}Na$, 791.2310).

4-β-D-Glucosyl-nogalamycinone (**6**). $C_{27}H_{28}O_{13}$ (560); yellow solid; *HPLC-*R_t = 15.54 min (Supporting Information, Figures S73 − S82); UV−vis λ_{max} 196, 226, 260, 286 (sh), 412 nm; ^{1}H NMR (CD_3OD, 600 MHz) and ^{13}C NMR (CD_3OD, 150 MHz), see Table S5; (−)-ESI-MS: m/z 559 [M − H]$^-$; (+)-ESI-MS: m/z 363 [(M-glucose-2H_2O) + H]$^+$; (−)-HRESI-MS: m/z 559.1459 [M − H]$^-$ (calcd for $C_{27}H_{27}O_{13}$, 559.1457); (+)-HRESI-MS: m/z 363.0860 [(M-glucose-2H_2O) + H]$^+$ (calcd for $C_{21}H_{15}O_6$, 363.0863).

■ ASSOCIATED CONTENT

Supporting Information

The Supporting Information is available free of charge at https://pubs.acs.org/doi/10.1021/acssynbio.2c00498.

> Experimental procedure for generation of *S. coelicolor* M1152Δ*matAB* strain, plasmid maps for vectors, sequences of BioBricks parts and coding sequences, high-resolution mass spectrometry data, NMR tables, NMR spectra, HPLC-UV−vis chromatograms, and dose−response data for human cancer cell lines (PDF)

■ AUTHOR INFORMATION

Corresponding Authors

Mikko Metsä-Ketelä − *Department of Life Technologies, University of Turku, FIN-20014 Turku, Finland;* orcid.org/0000-0003-3176-2908; Email: mianme@utu.fi

Khaled A. Shaaban − *Center for Pharmaceutical Research and Innovation and Department of Pharmaceutical Sciences, College of Pharmacy, University of Kentucky, Lexington, Kentucky 40536, United States;* orcid.org/0000-0001-7638-4942; Email: khaled_shaaban@uky.edu

S. Eric Nybo − *Department of Pharmaceutical Sciences, College of Pharmacy, Ferris State University, Big Rapids, Michigan 49307, United States;* orcid.org/0000-0001-7884-7787; Email: ericnybo@ferris.edu

Authors

Rongbin Wang − *Department of Life Technologies, University of Turku, FIN-20014 Turku, Finland*

Jennifer Nguyen − *Department of Pharmaceutical Sciences, College of Pharmacy, Ferris State University, Big Rapids, Michigan 49307, United States;* orcid.org/0000-0002-4557-1638

Jacob Hecht − *Department of Pharmaceutical Sciences, College of Pharmacy, Ferris State University, Big Rapids, Michigan 49307, United States*

Nora Schwartz − *Department of Pharmaceutical Sciences, College of Pharmacy, Ferris State University, Big Rapids, Michigan 49307, United States*

Katelyn V. Brown − *Department of Pharmaceutical Sciences, College of Pharmacy, Ferris State University, Big Rapids, Michigan 49307, United States*

Larissa V. Ponomareva − *Center for Pharmaceutical Research and Innovation and Department of Pharmaceutical Sciences, College of Pharmacy, University of Kentucky, Lexington, Kentucky 40536, United States*

Magdalena Niemczura − *Department of Life Technologies, University of Turku, FIN-20014 Turku, Finland*

Dino van Dissel − *Institute of Biology, Leiden University, 2333 BE Leiden, The Netherlands; Department of Biotechnology and Nanomedicine, SINTEF AS, NO-7465 Trondheim, Norway*

Gilles P. van Wezel − *Institute of Biology, Leiden University, 2333 BE Leiden, The Netherlands;* orcid.org/0000-0003-0341-1561

Jon S. Thorson − *Center for Pharmaceutical Research and Innovation and Department of Pharmaceutical Sciences, College of Pharmacy, University of Kentucky, Lexington, Kentucky 40536, United States;* orcid.org/0000-0002-7148-0721

Complete contact information is available at: https://pubs.acs.org/10.1021/acssynbio.2c00498

Author Contributions

¶R.W. and J.N. contributed equally to this work.

Notes

The authors declare the following competing financial interest(s): Material published in this report is covered under U.S. Patent Application No. 16/015,821 to Ferris State University.

https://doi.org/10.1021/acssynbio.2c00498
ACS Synth. Biol. 2022, 11, 4193−4209

■ ACKNOWLEDGMENTS

Research reported in this publication was supported by the National Science Foundation under Grant No. ENG-2015951 (S.E.N.), by the National Cancer Institute of the National Institutes of Health under Award No. R15CA252830 (S.E.N.), the NIGMS-supported Center of Biomedical Research Excellence (COBRE) in Pharmaceutical Research and Innovation (CPRI, NIH P20 GM130456), the University of Kentucky College of Pharmacy, the National Center for Advancing Translational Sciences (UL1TR000117 and UL1TR001998) and a National Institutes of Health shared instrumentation Grant (S10OD28690), Novo Nordisk Foundation Grant No. NNF19OC0057511 (to M.M.-K) and Academy of Finland Grant No. 340013 (to M.M.-K.). We also acknowledge a grant from the Turku University Foundation and support from the China Scholarship Council 202107960010 (R.W.). G.v.W. was funded by ERC Advanced grant 101055020 from the European Research Council. We thank the College of Pharmacy NMR Center (University of Kentucky) for NMR support. We thank Dr. Lou Charkoudian for the gift of strain *S. lividans* K4-114. We thank Prof. Dr. Mervyn Bibb for the gift of strains *S. coelicolor* M1146 and M1152. We thank Dr. Isaac Brownell (Dermatology Branch, National Cancer Institute, National Institutes of Health, Bethesda, MD, USA) for the gift of Merkel cells MKL1 and MCC26.

■ REFERENCES

(1) Hulst, M. B.; Grocholski, T.; Neefjes, J. J. C.; van Wezel, G. P.; Metsä-Ketelä, M. Anthracyclines: Biosynthesis, Engineering and Clinical Applications. *Nat. Prod. Rep.* **2022**, *39*, 814.

(2) Pang, B.; Qiao, X.; Janssen, L.; Velds, A.; Groothuis, T.; Kerkhoven, R.; Nieuwland, M.; Ovaa, H.; Rottenberg, S.; van Tellingen, O.; Janssen, J.; Huijgens, P.; Zwart, W.; Neefjes, J. Drug-Induced Histone Eviction from Open Chromatin Contributes to the Chemotherapeutic Effects of Doxorubicin. *Nat. Commun.* **2013**, *4* (1), 1−13.

(3) Rajgarhia, V. B.; Strohl, W. R. Minimal *Streptomyces* Sp. Strain C5 Daunorubicin Polyketide Biosynthesis Genes Required for Aklanonic Acid Biosynthesis. *J. Bacteriol.* **1997**, *179* (8), 2690−2696.

(4) Grimm, A.; Madduri, K.; Ali, A.; Hutchinson, C. R. Characterization of the *Streptomyces peucetius* ATCC 29050 Genes Encoding Doxorubicin Polyketide Synthase. *Gene* **1994**, *151* (1−2), 1−10.

(5) Torkkell, S.; Kunnari, T.; Palmu, K.; Mäntsälä, P.; Hakala, J.; Ylihonko, K. The Entire Nogalamycin Biosynthetic Gene Cluster of *Streptomyces nogalater*: Characterization of a 20-Kb DNA Region and Generation of Hybrid Structures. *Molecular Genetics and Genomics* **2001**, *266* (2), 276−288.

(6) Ylihonko, K.; Tuikkanen, J.; Jussila, S.; Cong, L.; Mäntsälä, P. A Gene Cluster Involved in Nogalamycin Biosynthesis from *Streptomyces nogalater*: Sequence Analysis and Complementation of Early-Block Mutations in the Anthracycline Pathway. *Molecular and General Genetics* **1996**, *251*, 113−120.

(7) Räty, K.; Kantola, J.; Hautala, A.; Hakala, J.; Ylihonko, K.; Mäntsälä, P. Cloning and Characterization of *Streptomyces galilaeus* Aclacinomycins Polyketide Synthase (PKS) Cluster. *Gene* **2002**, *293* (1−2), 115−122.

(8) Bao, W.; Sheldon, P. J.; Wendt-Pienkowski, E.; Hutchinson, C. R. The *Streptomyces peucetius* DpsC Gene Determines the Choice of Starter Unit in Biosynthesis of the Daunorubicin Polyketide. *J. Bacteriol.* **1999**, *181* (15), 4690−4695.

(9) Hautala, A.; Torkkell, S.; Räty, K.; Kunnari, T.; Kantola, J.; Mantsälä, P.; Hakala, J.; Ylihonko, K. Studies on a Second and Third Ring Cyclization in Anthracycline Biosynthesis. *J. Antibiot (Tokyo)* **2003**, *56* (2), 143−153.

(10) Chung, J.-y.; Fujii, I.; Harada, S.; Sankawa, U.; Ebizuka, Y. Expression, Purification, and Characterization of AknX Anthrone Oxygenase, Which Is Involved in Aklavinone Biosynthesis in *Streptomyces galilaeus*. *J. Bacteriol.* **2002**, *184* (22), 6115−6122.

(11) Kantola, J.; Kunnari, T.; Hautala, A.; Hakala, J.; Ylihonko, K.; Mäntsälä, P. Elucidation of Anthracyclinone Biosynthesis by Stepwise Cloning of Genes for Anthracyclines from Three Different *Streptomyces* Spp. *Microbiology (Reading)* **2000**, *146* (1), 155−163.

(12) Connors, N. C.; Bartel, P. L.; Strohl, W. R. Biosynthesis of Anthracyclines: Enzymic Conversion of Aklanonic Acid to Aklavinone and ϵ-Rhodomycinone by Anthracycline-Producing Streptomycetes. *J. Gen. Microbiol.* **1990**, *136*, 1887.

(13) Sultana, A.; Kallio, P.; Jansson, A.; Wang, J. S.; Niemi, J.; Mäntsälä, P.; Schneider, G. Structure of the Polyketide Cyclase SnoaL Reveals a Novel Mechanism for Enzymatic Aldol Condensation. *EMBO J.* **2004**, *23* (9), 1911−1921.

(14) Torkkell, S.; Kunnari, T.; Palmu, K.; Hakala, J.; Mantsala, P.; Ylihonko, K. Identification of a Cyclase Gene Dictating the C-9 Stereochemistry of Anthracyclines from *Streptomyces nogalater*. *Antimicrob. Agents Chemother.* **2000**, *44* (2), 396−399.

(15) Kallio, P.; Sultana, A.; Niemi, J.; Mäntsälä, P.; Schneider, G. Crystal Structure of the Polyketide Cyclase AknH with Bound Substrate and Product Analogue: Implications for Catalytic Mechanism and Product Stereoselectivity. *J. Mol. Biol.* **2006**, *357* (1), 210−220.

(16) Heinemann, M.; Panke, S. Synthetic Biology–Putting Engineering into Biology. *Bioinformatics* **2006**, *22* (22), 2790−2799.

(17) Tippmann, S.; Chen, Y.; Siewers, V.; Nielsen, J. From Flavors and Pharmaceuticals to Advanced Biofuels: Production of Isoprenoids in *Saccharomyces cerevisiae*. *Biotechnol J.* **2013**, *8* (12), 1435−1444.

(18) Yuzawa, S.; Backman, T. W. H.; Keasling, J. D.; Katz, L. Synthetic Biology of Polyketide Synthases. *J. Ind. Microbiol. Biotechnol.* **2018**, *45* (7), 621−633.

(19) van Dissel, D.; Claessen, D.; Roth, M.; van Wezel, G. P. A Novel Locus for Mycelial Aggregation Forms a Gateway to Improved *Streptomyces* Cell Factories. *Microb Cell Fact* **2015**, *14* (1), 44.

(20) Medema, M. H.; Breitling, R.; Takano, E. Synthetic Biology in *Streptomyces* Bacteria. *Methods Enzymol.* **2011**, *497*, 485−502.

(21) van Dissel, D.; Willemse, J.; Zacchetti, B.; Claessen, D.; Pier, G. B.; van Wezel, G. P. Production of Poly-β-1,6-N-Acetylglucosamine by MatAB Is Required for Hyphal Aggregation and Hydrophilic Surface Adhesion by *Streptomyces*. *Microbial Cell* **2018**, *5* (6), 269−279.

(22) Ylihonko, K.; Hakala, J.; Kunnari, T.; Mantsalala, P. Production of Hybrid Anthracycline Antibiotics by Heterologous Expression of *Streptomyces nogalater* Nogalamycin Biosynthesis Genes. *Microbiology (N Y)* **1996**, *142* (8), 1965−1972.

(23) Elowitz, M. B.; Leibler, S. A Synthetic Oscillatory Network of Transcriptional Regulators. *Nature* **2000**, *403* (6767), 335−338.

(24) Nguyen, J. T.; Riebschleger, K. K.; Brown, K. v.; Gorgijevska, N. M.; Nybo, S. E. A BioBricks Toolbox for Metabolic Engineering of the Tetracenomycin Pathway. *Biotechnol J.* **2022**, *17*, No. 2100371.

(25) Shetty, R. P.; Endy, D.; Knight, T. F. Engineering BioBrick Vectors from BioBrick Parts. *J. Biol. Eng.* **2008**, *2* (1), 5.

(26) Bierman, M.; Logan, R.; O'Brien, K.; Seno, E. T.; Nagaraja Rao, R.; Schoner, B. E. Plasmid Cloning Vectors for the Conjugal Transfer of DNA from *Escherichia coli* to *Streptomyces* Spp. *Gene* **1992**, *116* (1), 43−49.

(27) Flett, F.; Mersinias, V.; Smith, C. P.; Flett', F.; Mersinias, V.; Smith, C. P. High Efficiency Intergeneric Conjugal Transfer of Plasmid DNA from *Escherichia coli* to Methyl DNA-Restricting Streptomycetes. *FEMS Microbiol Lett.* **1997**, *155* (2), 223−229.

(28) Wang, W.; Li, X.; Wang, J.; Xiang, S.; Feng, X.; Yang, K. An Engineered Strong Promoter for Streptomycetes. *Appl. Environ. Microbiol.* **2013**, *79* (14), 4484−4492.

(29) Bai, C.; Zhang, Y.; Zhao, X.; Hu, Y.; Xiang, S.; Miao, J.; Lou, C.; Zhang, L.; Demain, A. L. Exploiting a Precise Design of Universal Synthetic Modular Regulatory Elements to Unlock the Microbial Natural Products in *Streptomyces*. *Proc. Natl. Acad. Sci. U. S. A.* **2015**, *112* (39), 12181−12186.

(30) Ziermann, R.; Betlach, M. C. Recombinant Polyketide Synthesis in *Streptomyces*: Engineering of Improved Host Strains. *Biotechniques* **1999**, *26* (1), 106−110.

https://doi.org/10.1021/acssynbio.2c00498
ACS Synth. Biol. 2022, 11, 4193−4209

(31) Gomez-Escribano, J. P.; Bibb, M. J. Engineering *Streptomyces coelicolor* for Heterologous Expression of Secondary Metabolite Gene Clusters. *Microb Biotechnol* **2011**, *4* (2), 207−215.
(32) Aubry, C.; Pernodet, J. L.; Lautru, S. Modular and Integrative Vectors for Synthetic Biology Applications in *Streptomyces* Spp. *Appl. Environ. Microbiol.* **2019**, DOI: 10.1128/AEM.00485-19.
(33) Siitonen, V.; Claesson, M.; Patrikainen, P.; Aromaa, M.; Mäntsälä, P.; Schneider, G.; Metsä-Ketelä, M. Identification of Late-Stage Glycosylation Steps in the Biosynthetic Pathway of the Anthracycline Nogalamycin. *ChemBioChem.* **2012**, *13* (1), 120−128.
(34) MacNeil, D. J.; Gewain, K. M.; Ruby, C. L.; Dezeny, G.; Gibbons, P. H.; MacNeil, T. Analysis of *Streptomyces avermitilis* Genes Required for Avermectin Biosynthesis Utilizing a Novel Integration Vector. *Gene* **1992**, *111* (1), 61−68.
(35) Liu, X.; Hua, K.; Liu, D.; Wu, Z. L.; Wang, Y.; Zhang, H.; Deng, Z.; Pfeifer, B. A.; Jiang, M. Heterologous Biosynthesis of Type II Polyketide Products Using *E. coli*. *ACS Chem. Biol.* **2020**, *15* (5), 1177−1183.
(36) Knight, T. Idempotent Vector Design for Standard Assembly of Biobricks Idempotent Vector Design for Standard Assembly of Biobricks. *Structure* **2003**, 1−11.
(37) Zhang, W.; Watanabe, K.; Wang, C. C. C.; Tang, Y. Heterologous Biosynthesis of Amidated Polyketides with Novel Cyclization Regioselectivity from Oxytetracycline Polyketide Synthase. *J. Nat. Prod* **2006**, *69* (11), 1633−1636.
(38) Wohlert, S. E.; Wendt-Pienkowski, E.; Bao, W.; Hutchinson, C. R. Production of Aromatic Minimal Polyketides by the Daunorubicin Polyketide Synthase Genes Reveals the Incompatibility of the Heterologous DpsY and JadI Cyclases. *J. Nat. Prod* **2001**, *64* (8), 1077−1080.
(39) Bibb, M. J.; Janssen, G. R.; Ward, J. M. Cloning and Analysis of the Promoter Region of the Erythromycin-Resistance Gene (ErmE) of *Streptomyces erythraeus*. *Gene* **1986**, *41* (2−3), E357.
(40) Nybo, S. E.; Saunders, J.; McCormick, S. P. Metabolic Engineering of *Escherichia coli* for Production of Valerenadiene. *J. Biotechnol.* **2017**, *262*, 60−66.
(41) Wardell, J. N.; Stocks, S. M.; Thomas, C. R.; Bushell, M.E. Decreasing the Hyphal Branching Rate of Saccharopolyspora Erythraea NRRL 2338 Leads to Increased Resistance to Breakage and Increased Antibiotic Production. *Biotechnol. Bioeng.* **2002**, *78* (2), 141−146.
(42) van Dissel, D.; Claessen, D.; van Wezel, G. P. Morphogenesis of Streptomyces in Submerged Cultures. *Adv. Appl. Microbiol.* **2014**, *89*, 1−45.
(43) van Wezel, G. P.; Krabben, P.; Traag, B.ør. A.; Keijser, B. J. F.; Kerste, R.; Vijgenboom, E.; Heijnen, J. J.; Kraal, B. Unlocking Streptomyces Spp. for Use as Sustainable Industrial Production Platforms by Morphological Engineering. *Appl. Environ. Microbiol.* **2006**, *72* (8), 5283−5288.
(44) Luo, Y.; Zhang, L.; Barton, K. W.; Zhao, H. Systematic Identification of a Panel of Strong Constitutive Promoters from *Streptomyces albus*. *ACS Synth. Biol.* **2015**, *4* (9), 1001−1010.
(45) Yang, D.; Jang, D.; Lee, S. Y. Production of Carminic Acid by Metabolically Engineered *Escherichia coli*. *Cite This: J. Am. Chem. Soc.* **2021**, *143*, 5364−5377.
(46) Ji, C. H.; Kim, J. P.; Kang, H. S. Library of Synthetic *Streptomyces* Regulatory Sequences for Use in Promoter Engineering of Natural Product Biosynthetic Gene Clusters. *ACS Synth. Biol.* **2018**, *7*, 1946−1955.
(47) Kendrew, S. G.; Katayama, K.; Deutsch, E.; Madduri, K.; Hutchinson, C. R. DnrD Cyclase Involved in the Biosynthesis of Doxorubicin: Purification and Characterization of the Recombinant Enzyme †. *Biochemistry* **1999**, *38* (15), 4794−4799.
(48) Gaspar, P.; Oliveira, J. L.; Frommlet, J.; Santos, M. A. S.; Moura, G. EuGene: Maximizing Synthetic Gene Design for Heterologous Expression. *Bioinformatics* **2012**, *28* (20), 2683−2684.
(49) Al-Hawash, A. B.; Zhang, X.; Ma, F. Strategies of Codon Optimization for High-Level Heterologous Protein Expression in Microbial Expression Systems. *Gene Rep* **2017**, *9*, 46−53.
(50) Hu, S.; Wang, M.; Cai, G.; He, M. Genetic Code-Guided Protein Synthesis and Folding in *Escherichia coli*. *J. Biol. Chem.* **2013**, *288* (43), 30855−30861.
(51) Sander, I. M.; Chaney, J. L.; Clark, P. L. Expanding Anfinsen's Principle: Contributions of Synonymous Codon Selection to Rational Protein Design. *J. Am. Chem. Soc.* **2014**, *136* (3), 858−861.
(52) Gui, C.; Chen, J.; Xie, Q.; Mo, X.; Zhang, S.; Zhang, H.; Ma, J.; Li, Q.; Gu, Y. C.; Ju, J. CytA, a Reductase in the Cytorhodin Biosynthesis Pathway, Inactivates Anthracycline Drugs in *Streptomyces*. *Commun. Biol.* **2019**, DOI: 10.1038/s42003-019-0699-5.
(53) Arora, S. K. Structure of Aklavinone, a DNA Binding Anthracycline Antibiotic. *J. Antibiot (Tokyo)* **1985**, *38* (12), 1788−1791.
(54) Fujiwara, A.; Hoshino, T.; Tazoe, M.; Fujiwara, M. Auramycins and Sulfurmycins, New Anthracycline Antibiotics: Characterization of Aglycones, Auramycinone and Sulfurmycinone. *J. Antibiot (Tokyo)* **1981**, *34* (5), 608−610.
(55) Muroi, T.; Kokuzawa, T.; Kihara, Y.; Kobayashi, R.; Hirano, N.; Takahashi, H.; Haruki, M. TG1 Integrase-Based System for Site-Specific Gene Integration into Bacterial Genomes. *Appl. Microbiol. Biotechnol.* **2013**, *97* (9), 4039−4048.
(56) Morita, K.; Yamamoto, T.; Fusada, N.; Komatsu, M.; Ikeda, H.; Hirano, N.; Takahashi, H. The Site-Specific Recombination System of Actinophage TG1. *FEMS Microbiol Lett.* **2009**, *297* (2), 234−240.
(57) Adnani, N.; Chevrette, M. G.; Adibhatla, S. N.; Zhang, F.; Yu, Q.; Braun, D. R.; Nelson, J.; Simpkins, S. W.; McDonald, B. R.; Myers, C. L.; Piotrowski, J. S.; Thompson, C. J.; Currie, C. R.; Li, L.; Rajski, S. R.; Bugni, T. S. Coculture of Marine Invertebrate-Associated Bacteria and Interdisciplinary Technologies Enable Biosynthesis and Discovery of a New Antibiotic, Keyicin. *ACS Chem. Biol.* **2017**, *12*, No. 3093.
(58) Gentz, R.; Langner, A.; Chang, A. C. Y.; Cohen, S. N.; Bujard, H. Cloning and Analysis of Strong Promoters Is Made Possible by the Downstream Placement of a RNA Termination Signal. *Proc. Natl. Acad. Sci. U. S. A.* **1981**, *78* (8), 4936−4940.
(59) Otsuka, J.; Kunisawa, T. Characteristic Base Sequence Patterns of Promoter and Terminator Sites in ΦX174 and Fd Phage DNAs. *J. Theor. Biol.* **1982**, *97* (3), 415−436.
(60) Huff, J.; Czyz, A.; Landick, R.; Niederweis, M. Taking Phage Integration to the next Level as a Genetic Tool for *Mycobacteria*. *Gene* **2010**, *468* (1−2), 8−19.
(61) Zhao, M.; Wang, M.; Wang, S.; Xiong, L.; Gao, B.; Liu, M.; Tao, X.; Wang, F.-Q.; Wei, D. A Self-Sustained System Spanning the Primary and Secondary Metabolism Stages to Boost the Productivity of *Streptomyces*. *ACS Synth. Biol.* **2022**, *11*, 353-365.
(62) Li, L.; Zheng, G.; Chen, J.; Ge, M.; Jiang, W.; Lu, Y. Multiplexed Site-Specific Genome Engineering for Overproducing Bioactive Secondary Metabolites in Actinomycetes. *Metab Eng.* **2017**, *40*, 80−92.
(63) Siegl, T.; Tokovenko, B.; Myronovskyi, M.; Luzhetskyy, A. Design, Construction and Characterisation of a Synthetic Promoter Library for Fine-Tuned Gene Expression in Actinomycetes. *Metab. Eng.* **2013**, *19*, 98-106.
(64) Siitonen, V.; Selvaraj, B.; Niiranen, L.; Lindqvist, Y.; Schneider, G.; Metsä-Ketelä, M. Divergent Non-Heme Iron Enzymes in the Nogalamycin Biosynthetic Pathway. *Proc. Natl. Acad. Sci. U. S. A.* **2016**, *113* (19), 5251.
(65) Grocholski, T.; Yamada, K.; Sinkkonen, J.; Tirkkonen, H.; Niemi, J.; Metsä-Ketelä, M. Evolutionary Trajectories for the Functional Diversification of Anthracycline Methyltransferases. *ACS Chem. Biol.* **2019**, *14* (5), 850−856.
(66) Brown, K. V.; Wandi, B. N.; Metsa-Ketela, M.; Nybo, S. E. Pathway Engineering of Anthracyclines: Blazing Trails in Natural Product Glycodiversification. *J. Org. Chem.* **2020**, *85* (19), 12012−12023.
(67) Leng, F.; Savkur, R.; Fokt, I.; Przewloka, T.; Priebe, W.; Chaires, J. B. Base Specific and Regioselective Chemical Cross-Linking of Daunorubicin to DNA. *J. Am. Chem. Soc.* **1996**, *118* (20), 4731−4738.
(68) Fu, H.; McDaniel, R.; Hopwood, D. A.; Khosla, C. Engineered Biosynthesis of Novel Polyketides: Stereochemical Course of Two

Reactions Catalyzed by a Polyketide Synthase. *Biochemistry* **1994**, *33* (31), 9321−9326.
(69) McDaniel, R.; Ebert-Khosla, S.; Hopwood, D. A.; Khosla, C. Engineered Biosynthesis of Novel Polyketides: Manipulation and Analysis of an Aromatic Polyketide Synthase with Unproven Catalytic Specificities. *J. Am. Chem. Soc.* **1993**, *115* (25), 11671−11675.
(70) McDaniel, R.; Ebert-Khosla, S.; Fu, H.; Hopwood, D. A.; Khosla, C. Engineered Biosynthesis of Novel Polyketides: Influence of a Downstream Enzyme on the Catalytic Specificity of a Minimal Aromatic Polyketide Synthase. *Proc. Natl. Acad. Sci. U. S. A.* **1994**, *91* (24), 11542−11546.
(71) McDaniel, R.; Ebert-Khosla, S.; Hopwood, D. A.; Khosla, C. Engineered Biosynthesis of Novel Polyketides. *Science* **1993**, *262* (5139), 1546−1550.
(72) McDaniel, R.; Khosla, C.; Hutchinson, C. R. Engineered Biosynthesis of Novel Polyketides: Analysis of TcmN Function in Tetracenomycin Biosynthesis. *J. Am. Chem. Soc.* **1995**, *117* (26), 6805−6810.
(73) Weissman, K. J.; Leadlay, P. F. Combinatorial Biosynthesis of Reduced Polyketides. *Nat. Rev. Microbiol.* **2005**, *3*, 925−936.
(74) Weissman, K. J. Genetic Engineering of Modular PKSs: From Combinatorial Biosynthesis to Synthetic Biology. *Nat. Prod Rep* **2016**, *33* (2), 203−230.
(75) Pahari, P.; Kharel, M. K.; Shepherd, M. D.; van Lanen, S. G.; Rohr, J. Enzymatic Total Synthesis of Defucogilvocarcin M and Its Implications for Gilvocarcin Biosynthesis. *Angew. Chem., Int. Ed. Engl.* **2012**, *51* (5), 1216−1220.
(76) Wang, G.; Chen, J.; Zhu, H.; Rohr, J. One-Pot Enzymatic Total Synthesis of Presteffimycinone, an Early Intermediate of the Anthracycline Antibiotic Steffimycin Biosynthesis. *Org. Lett.* **2017**, *19* (3), 540−543.
(77) Poust, S.; Hagen, A.; Katz, L.; Keasling, J. D. Narrowing the Gap between the Promise and Reality of Polyketide Synthases as a Synthetic Biology Platform. *Current Opinion in Biotechnology.* **2014**, *30*, 32−39.
(78) Blanchard, S.; Thorson, J. S. Enzymatic Tools for Engineering Natural Product Glycosylation. *Curr. Opin Chem. Biol.* **2006**, *10* (3), 263−271.
(79) Williams, G. J.; Zhang, C.; Thorson, J. S. Expanding the Promiscuity of a Natural-Product Glycosyltransferase by Directed Evolution. *Nat. Chem. Biol.* **2007**, *3* (10), 657−662.
(80) Williams, G. J.; Goff, R. D.; Zhang, C.; Thorson, J. S. Optimizing Glycosyltransferase Specificity via "Hot Spot" Saturation Mutagenesis Presents a Catalyst for Novobiocin Glycorandomization. *Chem. Biol.* **2008**, *15* (4), 393−401.
(81) Gantt, R. W.; Peltier-Pain, P.; Singh, S.; Zhou, M.; Thorson, J. S. Broadening the Scope of Glycosyltransferase-Catalyzed Sugar Nucleotide Synthesis. *Proc. Natl. Acad. Sci. U. S. A.* **2013**, *110* (19), 7648−7653.
(82) Hulst, M. B.; Grocholski, T.; Neefjes, J. J. C.; van Wezel, G. P.; Metsä-Ketelä, M. Anthracyclines: Biosynthesis, Engineering and Clinical Applications. *Nat. Prod. Rep.* **2022**, *39*, 814.
(83) Komatsu, Y.; Takahashi, O.; Hayashi, H. Identification of the Anthracycline Antibiotic 4-O-(*β*-D-Glucopyranuronosyl)-*ε*-Rhodomycinone, Produced by *Streptomyces ruber* JCM3131, as an Up-Regulator of MHC Class-I Molecules in B16/BL6 Cells. *J. Antibiot (Tokyo)* **1998**, *51* (1), 85−88.
(84) Sambrook, J.; W Russell, D. *Molecular Cloning: A Laboratory Manual*; Cold Spring Harbor Laboratory Press: Cold Spring Harbor, NY, 2001; p 999.
(85) Kieser, T.; Bibb, M. J.; Buttner, M. J.; Chater, K. F.; Hopwood, D. A. *Practical Streptomyces Genetics*; John Innes Centre Ltd., 2000; p 529. DOI: 10.4016/28481.01
(86) Ylihonko, K.; Hakala, J.; Niemi, J.; Lundell, J.; Mantsala, P. Isolation and Characterization of Aclacinomycin A-Non-Producing *Streptomyces galilaeus* (ATCC 31615) Mutants. *Microbiology (N Y)* **1994**, *140* (6), 1359−1365.
(87) Savi, D. C.; Shaaban, K. A.; Gos, F. M. W. R.; Ponomareva, L. V.; Thorson, J. S.; Glienke, C.; Rohr, J. Phaeophleospora Vochysiae Savi & Glienke Sp. Nov. Isolated from *Vochysia divergens* Found in the Pantanal, Brazil, Produces Bioactive Secondary Metabolites OPEN. *Sci. Rep.* **2018**, *8*, 3122.
(88) Shaaban, K. A.; Elshahawi, S. I.; Wang, X.; Horn, J.; Kharel, M. K.; Leggas, M.; Thorson, J. S. Cytotoxic Indolocarbazoles from *Actinomadura melliaura* ATCC 39691. *J. Nat. Prod.* **2015**, *78* (7), 1723−1729.
(89) Wang, X.; Shaaban, K. A.; Elshahawi, S. I.; Ponomareva, L. v; Sunkara, M.; Zhang, Y.; Copley, G. C.; Hower, J. C.; Morris, A. J.; Kharel, M. K.; Thorson, J. S. Frenolicins C−G, Pyrananophthoquinones from *Streptomyces* Sp. RM-4-15. *J. Nat. Prod.* **2013**, *76* (8), 1441-1447.
(90) Shaaban, K. A.; Wang, X.; Elshahawi, S. I.; Ponomareva, L. v.; Sunkara, M.; Copley, G. C.; Hower, J. C.; Morris, A. J.; Kharel, M. K.; Thorson, J. S. Herbimycins D-F, Ansamycin Analogues from *Streptomyces* Sp. RM-7−15. *J. Nat. Prod.* **2013**, *76* (9), 1619−1626.

Recommended by ACS

MGCEP 1.0: A Genetic-Engineered Marine-Derived Chassis Cell for a Scaled Heterologous Expression Platform of Microbial Bioactive Metabolites
Zhijie Yang, Junying Ma, *et al.*
OCTOBER 14, 2022
ACS SYNTHETIC BIOLOGY
READ

Discovery and Heterologous Expression of Microginins from *Microcystis aeruginosa* LEGE 91341
Nádia Eusébio, Pedro N. Leão, *et al.*
SEPTEMBER 27, 2022
ACS SYNTHETIC BIOLOGY
READ

A Toolkit for Precise, Multigene Control in *Saccharomyces cerevisiae*
Adam Sanford, Ahmad S. Khalil, *et al.*
NOVEMBER 11, 2022
ACS SYNTHETIC BIOLOGY
READ

High Titer of (*S*)-Equol Synthesis from Daidzein in *Escherichia coli*
Hanning Deng, Jingwen Zhou, *et al.*
OCTOBER 25, 2022
ACS SYNTHETIC BIOLOGY
READ

Get More Suggestions >